Journal of Minerals and Materials Characterization and Engineering, 2025, 13(4), 123-155
https://www.scirp.org/journal/jmmce
ISSN Online: 2327-4085
ISSN Print: 2327-4077

Hydrothermal Alteration in Diénéméra-Gongondy Paleoproterozoic Porphyry Copper Deposit, Burkina Faso, West African Craton

Aristide Belemsobgo[1,2*], Wendkouni Passecdé Pauline Zongo[1,3], Bepowo Hien[4], Urbain Wenmenga[1], Séta Naba[1]

[1]Laboratory of Geosciences and Environment, University Joseph Ki-Zerbo, Ouagadougou, Burkina Faso
[2]General Directorate of Mines and Geology, Ministry of Energy, Mines and Quarries, Ouagadougou, Burkina Faso
[3]Unviersity Lédéa Bernard Ouedraogo, Ouahygouya, Burkina Faso
[4]Department of Earth Resources Engineering, Faculty of Engineering, Kyushu University, Kyushu, Japan
Email: *belaris1er@yahoo.fr

How to cite this paper: Belemsobgo, A., Zongo, W.P.P., Hien, B., Wenmenga, U. and Naba, S. (2025) Hydrothermal Alteration in Diénéméra-Gongondy Paleoproterozoic Porphyry Copper Deposit, Burkina Faso, West African Craton. *Journal of Minerals and Materials Characterization and Engineering*, **13**, 123-155.
https://doi.org/10.4236/jmmce.2025.134009

Received: February 6, 2025
Accepted: July 1, 2025
Published: July 4, 2025

Copyright © 2025 by author(s) and Scientific Research Publishing Inc.
This work is licensed under the Creative Commons Attribution International License (CC BY 4.0).
http://creativecommons.org/licenses/by/4.0/
Open Access

Abstract

Diénéméra-Gongondy copper-gold deposit is one of the rare Paleoproterozoic porphyry copper deposit of West African Craton. Like most of the Precambrian porphyry copper deposits, the mineralization of Diénéméra-Gongondy copper-gold deposit still remains controversial. In this study, we used thirteen drill cores of "Projet Minier Gaoua" to characterize the petrographic, geochemical signature and ore mineralogy. However, δ34S isotopic analyses has been also conducted on these samples in order to determine the source of fluids associated to the Diénéméra-Gongondy copper-gold deposit. Macroscopic and microscopic observations revealed a complex lithology encompassing a wide range of subvolcanic to volcano-plutonic rocks variable in mineralogy and texture, dominated by several facies of microdiorites which host the mineralization. This mineralization is affected by several phases of hydrothermal alteration dominated at Diénéméra by propylitization. However, at Gongondy, phyllitic-carbonate alteration type is dominant. The geochemical study of alteration minerals confirmed the presence of these alterations, but the potassic alteration is absent, probably destroy by late alteration events or retrograde metamorphism. The δ34S isotopic analyses on pyrite form four samples of pyrite and chalcopyrite of Diénéméra and Gongondy deposits showed that the δ34S values range from −4.1 to 4.7. These values are in accordance with a magmatic origin of the sulfide, with a probable little contribution of late hydrothermal or meteoritic fluids. The (Cs + Rb)/Th normalized diagram con-

firms the potential mineralization of Diénéméra and Gongondy deposits, whereas the excess Aluminum diagram is confident for a porphyry type of mineralization. In definitive, all the results show that the Diénéméra-Gongondy copper-gold deposit is a porphyry type of birimian age affected by late stage magmatic, structural and hydrothermal events.

Keywords

West African Craton, Birimian, Porphyry Copper, Hydrothermal Alteration

1. Introduction

Porphyry copper is a copper, gold and molybdenum mineralization with low grade to high tonnage. The mineralization represents 50 - 60wt.% of copper, 95wt.% of Molybdenum production in the world and other by-product minerals including gold, silver, tungsten, tin. The mineralization is associated with some complex porphyritic intrusions with intermediate to mafic compositions, emplaced at depth of 2 km - 4 km [1] [2]. The deposits are generally associated with subduction zones, preferentially in continental arcs where the crust thickness favors the formation of the mineralization [3]-[5].

Most of the giant porphyry copper deposits are located in Circum Pacific magmatic arc, a relatively young continental arc with a great thickness. The most important criteria for the genesis of porphyry copper, are the fugacity of O_2 in the magma, the degree of fractionation of intrusive rocks (high Sr/Y) and the evolution of magmatic-hydrothermal fluid [6]-[12].

In West African Craton (WAC), some porphyry copper deposits are presents, associated with greenstones belts, the most prolific Paleoproterozoic gold province in the world with an average 10,000-metric ton of gold endowment [13]. This omnipresence of orogenic gold deposits in the WAC can be subject to confusion or superposition with other types of mineralization present in the WAC including Iron Oxide Copper Gold [14], Skarns [15]-[17], intrusion-related [18]-[20] and porphyry copper [21]-[33].

In Diénéméra-Gongondy porphyry copper deposit, the characteristic of the copper mineralization is in accordance with porphyry style [22]-[24] which is overprinted by a late orogenic gold mineralization [28] [29] [31]. In this deposit, the great part of the economic copper mineralization (>0.5wt% Cu) is linked with hydrothermal breccia which affects the intrusion complex [24], notably in the contact between andesite and diorite [29]-[31]. The breccia is 200 - 500 metres wide at surface and extend downwards to a maximum of 330 metres. They dip at 50˚ - 70˚ west in the Eastern part in Diénéméra, but in the western part, the dip of the breccia is subvertical and complexly scalloped at the southern end of the Gongondy deposit. They are generally monolithic and show abundant clasts (clasts-hosted type). The reduced matrix is composed of hydrothermal minerals domi-

nated by quartz, K-feldspar, epidote, chlorite, amphibolite, magnetite, calcite and anhydrite. Chalcopyrite and pyrite are the main sulfide minerals and are found in the breccia intra-clasts, generally associated with gold, minor bornite and molybdenite. The copper and gold content of the hydrothermal breccia varies greatly and is between 0.2 to 2wt% for copper. The most important copper mineralization is observed when the matrix become more abundant [23] [24]. Outside of hydrothermal breccia, the copper and gold mineralization decreases considerably with a copper grade between 0.1 to 0.2wt%. In these areas, the mineralization is typically disseminated or in form of stockwork veins (calcite-chalcopyrite, epidote-chalcopyrite, anhydrite-chalcopyrite veinlets) with minor gold [24] [31].

At Gongondy, economic mineralization infers an orebody of 300 to 700 metres wide that is continuous for about 900 to 2000 metres long and extending from 150 to 500 metres downdip. At Diénéméra, the mineralization varies between 100 and 600 metres in width extending continuously between 400 and 1000 metres long, with a depth ranging from 200 to 400 metres [29] [31] [34]. Diénéméra-Gongondy Cu-Au mineralization lacks significant supergene enrichment, even if between 1929 and 1940, 5000 tons of ore grading 4 - 40wt% of copper was mined in Gongondy deposit in the form of chalcocite in the intersection between two inferred fractures zones [22] [35]. Minor oxided copper occur in the two deposits and consists of chalcocite, bornite, malachite, chrysocolla and rare azurite and cuprite [24]-[36]. The total indicated resource was established in Diénéméra and Gongondy deposits which have a total indicated resources of Diénéméra and Gongondy deposits estimated at 22 million metric tons at 0.29wt% Cu and 0.33 ppm of Au, whereas the total inferred resources of the two deposits is estimated at 282 Mt at 0.32wt% Cu for 0.35 ppm Au [34].

Although many studies have been carried out in the Gaoua porphyry copper deposit, the role of the hydrothermal alteration in the formation and evolution of the mineralization has not been clearly established. Most of the studies associated the mineralization with propylitic alteration minerals including chlorite, carbonates, epidote, quartz, white micas [23] [25] [27] [29]. In addition to the propylitic alteration, local potassic and sericitic alterations are distinguished in the study area [30]. Regarding the importance of hydrothermal alteration in the formation of porphyry copper deposit, this study aims to contribute to a better understanding of the hydrothermal alteration in the formation and evolution of the Gaoua (Diénéméra-Gongondy) Cu-Au deposit.

2. Geological Settings

The Diénéméra-Gongondy Cu-Au mineralization is located in the Man-Leo shield, in the southern part of the West African Craton (**Figure 1**). On the basis of the geology, the shield is divided into two domains. The western part is dominated by Archean rocks [37], marked by an important deformation and granitization defined by plutonic and metamorphic terranes dated between 3500 and 2900 Ma and separated from Paleoproterozoic terranes by the Sassandra fault.

These Paleoproterozoic terranes are formed by the Eburnean orogeny between 2200 and 2000 Ma. In Burkina Faso, these terranes represent about 86% of the country and dominated by volcano-sedimentary rocks delimitated by Eburnean batholiths and associated with several generations of granitoïd and mafic intrusions. Most of the Volcano-sedimentary rocks form belts trending NNE-SSW in the western part of the country, and NE-SW in the eastern part. The Diénéméra-Gongondy Cu-Au mineralization occurs in one of these belts, the Boromo greenstone belt (**Figure 2(A)**). The belt consists of thick basal mafic tholeiitic rocks (Basalt, gabbro) intercalated by detrital or chemical sediments, volcanoclastics and calc-alkaline volcanic rocks (andesite, dacite, rhyolite) [39] [40].

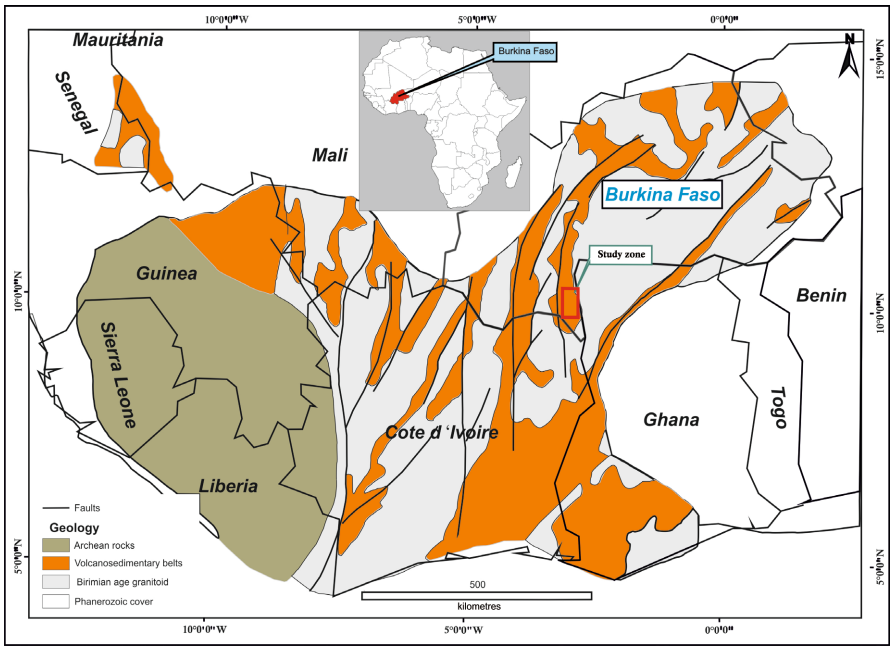

Figure 1. Localization of study zone in Man-Leo Shield [38].

In line with the geology of the WAC, the geology of Diénéméra-Gongondy Cu-Au mineralization consists of an association of volcanic and volcaniclastic rocks crosscut by various intrusions [23] [25] [41] [42].

Volcanic rocks are predominated by basalts and andesites forming pyroclastic flows, tuffs, dacitic or rhyolitic dykes. Basalt with a microlitic, porphyritic or pillow lavas texture, outcrops in the East and Northeast of Gaoua town [30] [39] [42]. Whereas, andesitic rocks are intercalated with volcano-sedimentary and volcanoclastic rocks and are locally brecciated, particularly in Diénéméra-Gongondy deposit [30]. Their frequent association with diorite in the zone, makes them difficultly distinguishable at macroscopic scale, particularly when they are altered.

The Diénéméra-Gongondy Cu-Au mineralization is hosted by subvolcanic intrusions which form an elongated volcano-plutonic complex oriented N-S (**Figure 2(B)**). The main rocks of this complex consist of quartz diorite and porphyry microdiorites with a large variety of textures, including intersertal, spherulitic,

ophitic textures [23] [25] [43]. Quartz diorites form some small lenticular intrusions in Diénéméra and circular bodies in Gongondy covering areas of few tens to one hundred square meters. Microdiorite porphyry also occurs as small intrusions in mafic rocks and is frequently crosscut by small albitic microgranite dykes [25].

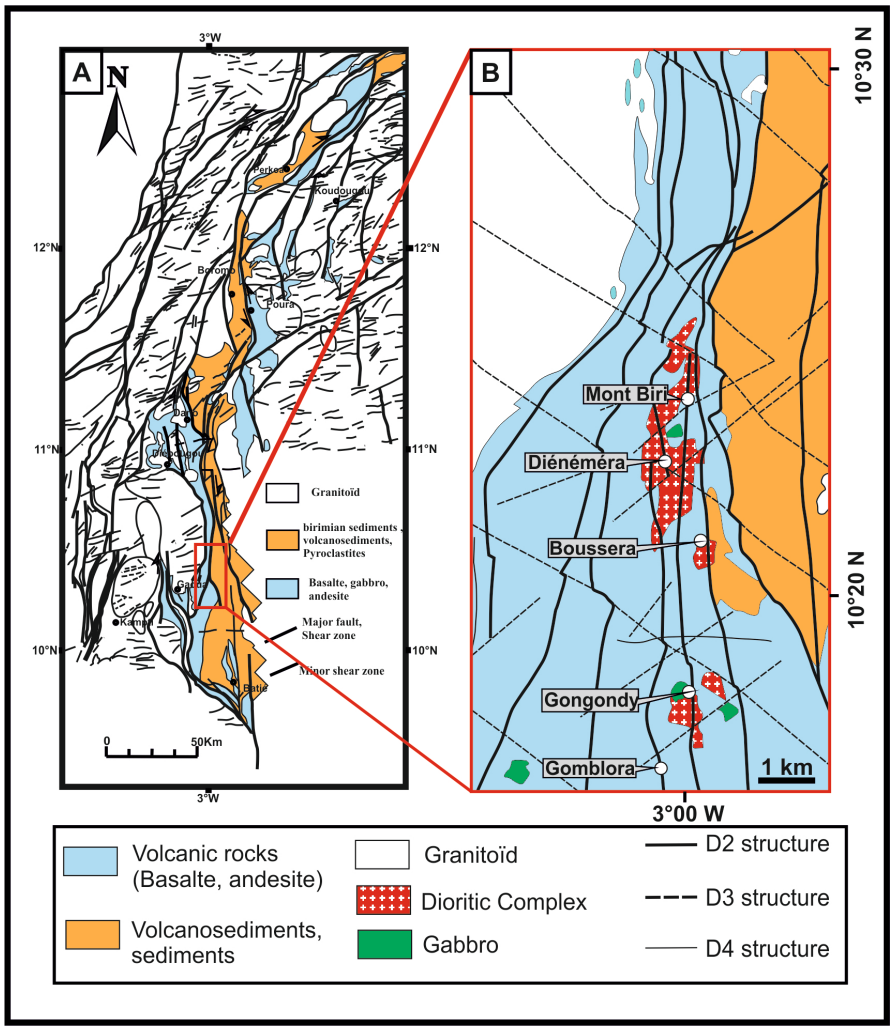

Figure 2. Localization of study zone in Boromo greenstone belt modified from [39] (A). Detailed geology of Diénéméra-Gongondy copper-gold deposits showing the dioritic complex according to [30] (B).

Some intrusions also occur in the basaltic rocks dated at 2171.6 ± 9.3 Ma using U-Pb method in the Gongondy prospect [44]. The volcano-plutonic complex locally occurs in the vicinity of the Gaoua batholith, a N-S elongated non-deformed calc-alkaline granite. Four deformation events are locally observed in the study area [30]. The late regional D1 [39] was not observed in the deposit scale, but some local deformations affect the main hosted rocks. The D1Ga deformation event is marked by N-S shortening observed in E-W trending mafic rocks near the Gaoua batholith.

A second deformation phase D2Ga occurred under greenschist facies, responsible of penetrative metamorphic foliation and folding under overall E-W compression. The late stage of this deformation event consists of a transcurrent regime characterized by intense N to NW-trending steeply dipping shear zones. During subsequent D3Ga, a network of brittle to brittle-ductile NW and NE faults were developed. The last deformation event D4Ga resulted in E-W trending thrust faults and crenulation cleavage planes, under overall N-S compression.

3. Materials and Methods

3.1. Data Acquisition and Sampling

The data of this study were acquired from Burkina Faso national geological survey. It consists of twelve drill cores from "Projet Minier Gaoua" (PMG) studies between 1982 and 1985. The drill cores were logged and one hundred and ten representative samples were taken in regards with the previous PMG geochemical copper anomaly contour, lithology, hydrothermal variation and mineralization type. The samples were described, labelled and put in some bags for further several laboratories studies.

3.2. Microscopic Studies

Polished thin sections were done in the laboratory of Geosciences and Environment, in the department of Earth Sciences of University Joseph KI-ZERBO and Burkina Faso national geological survey (BUMIGEB). We used a polarizing and metallographic microscope for sample description and analyses.

3.3. Geochemical Analysis of Whole Rock

Twenty-nine rock samples were analyzed for whole rock geochemistry. Sixteen samples were crushed in Bigs Global laboratory in Burkina Faso, before being sent eleven to Bureau Veritas laboratory in Canada and five in "Laboratoire Magmas et Volcans" (France) for whole rock analysis (Table 1 and Table 2).

Table 1. Major and traces elements of geochemical results of whole rock analyses.

Sample	E2G	E45G	E48G	E33G	EAL	B1	21-08	E2D	E43D	E42D	E8G	E17G	E18G	G4	G24/7
Facies	Porphyry microdiorite							Quartz porphyry microdiorite			Ophitic microdiorite		Microgabbro-diorite	Andesite	
Major elements (%)															
SiO_2	59.37	60.19	61.28	55.85	58.12	58	57.7	60.45	62.43	59.17	54.55	56.46	49.64	54.3	57.7
Al_2O_3	15.08	13.38	16.05	13.08	11.23	15.3	15.6	15.26	15.7	14.26	13.61	15	11.84	14.95	14.3
Fe_2O_3	8.12	9.69	7.64	8.86	20.23	7.6	9.38	7.15	7.12	13.61	6.55	5.68	6.98	6.36	9.73
CaO	2.14	0.3	0.58	5.02	0.22	7.31	4.89	6.15	3.35	2.42	5.76	4.77	7.54	5.12	3.11
MgO	4.59	2.06	4.03	2.32	2.02	4.35	4.03	3.16	2.3	1.1	6.21	3.62	6.51	3.53	5.18
Na_2O	3.6	2.99	3.64	0.84	0.19	3.85	3.6	3.85	4.57	4.87	3.76	5.63	3.33	4.54	2.29

Continued

K_2O	1.07	1.4	1.8	3.39	1.04	0.35	1.12	0.34	1.83	1.17	0.22	0.24	0.39	1.11	1.64
Cr_2O_3	0.019	-	-	-	-	0.03	0.02	0.01	0.009	-	0.044	0.005	0.036	0.02	0.04
TiO_2	0.49	0.46	0.53	0.35	0.37	0.5	0.54	0.44	0.39	0.41	0.76	0.64	0.6	0.77	0.47
MnO	0.04	0.06	0.03	0.06	0.06	0.09	0.18	0.06	0.02	0.03	0.1	0.08	0.14	0.09	0.06
P_2O_5	0.09	0.11	0.12	0.06	0.1	0.07	0.09	0.09	0.08	0.09	0.35	0.36	0.32	0.5	0.08
LOI	5	7.96	4.11	9.36	5.44	2.2	2.65	2.9	1.9	2.68	7.9	7.3	12.4	6.18	5.14
Traces elements (ppm)															
Ni	42	-	-	-	-	-	-	35	24	-	150	31	131		
Sc	20	12.4	16.9	17.5	16.6	-	-	15	12	13.8	16	13	21		
Ba	130	135.87	163.46	457.48	185.31	166.5	323	94	139	260.18	60	163	222	739	644
Be	2	0.58	0.68	0.67	0.45	-	-	<1	<1	0.61	<1	<1	1		
Co	28.2	94	103.49	75.8	56.9	62	27.2	12.3	9.5	444.32	25.1	16.7	29.4	24	29.7
Cs	1.2	1.55	1.8	1.96	1.84	1.43	1.25	0.5	2.3	1.66	0.6	0.4	1.2	1.14	2.05
Ga	14.4	14.9	20.1	13	16.4	17.2	16.4	15.1	15.2	17.1	14.3	16	13.7	19.9	18.1
Hf	1.8	1.78	2.58	1.71	1.56	2.1	2.3	1.6	1.8	1.82	3.3	3.6	2.7	4.5	2
Nb	2.2	2.96	3.57	2.09	2.04	1.8	3.5	1.6	1.1	2.47	4.5	3.8	2.7	8.4	3.4
Rb	27.2	38.4	51	70	20.3	10.6	29.4	9	67.2	42.6	6	6	10.6	36.9	53
Sn	<1	1.83	1.13	3.32	1.48	1	-	<1	1	1.09	<1	<1	<1	1	1
Sr	81.9	92.2	81.8	92.8	40.9	371	207	482.7	160.2	324.76	247.7	576	496.2	349	102.5
Ta	0.3	0.19	0.26	0.15	0.14	0.2	0.2	0.1	<0.1	0.15	0.4	0.2	0.2	0.7	0.2
Th	0.8	0.83	1.06	0.8	0.59	0.61	0.94	1	0.6	0.39	3.9	3.3	2.4	4	0.68
U	1.1	0.86	1.4	0.57	0.44	0.22	0.42	0.4	0.5	1.12	1.2	1.4	0.7	1.76	0.49
V	158	101.43	122.71	111.64	120.06	145	162	111	112	124.72	96	105	118	134	170
W	1.3	4.1	1.77	9.45	2.93	218	1	0.8	<0.5	2.06	0.7	0.6	<0.5	30	1
Zr	69.5	68.7	98.9	66.4	60.9	80	75	65.5	72.6	69.7	135.8	141.8	105.3	159	62
Y	10.7	16.2	12.4	7.83	11.4	11.6	12.5	7.9	7.3	17.2	10.4	13.6	13.2	17.6	10.2
La	8.8	5.65	4.24	7.95	3.49	6.3	8	5.1	5	10.9	29.2	28.3	21.8	34.8	2.9
Ce	16.1	12.6	8.84	20.1	8.03	14.5	17.3	12.1	10.1	23.3	56.1	59.4	48.1	75	6.7
Pr	2.13	1.67	1.11	2.9	1.11	1.98	2.31	1.72	1.35	2.79	7.11	7.55	6.52	9.7	1.03
Nd	7.7	7.32	4.69	12.8	4.84	8.7	10.2	6.9	6	10.4	30.2	28.3	27.4	39.4	5.2
Sm	1.96	1.81	1.13	2.88	1.33	2.16	2.07	1.72	1.33	1.94	4.82	5.99	5.68	7.56	1.42
Eu	0.6	0.68	0.47	1.03	0.5	0.71	0.8	0.54	0.46	0.63	1.21	1.6	1.6	2.18	0.46
Gd	2.03	2.34	1.47	2.09	1.83	2	2.46	1.57	1.18	2.22	3.62	4.51	4.31	6.75	1.51
Tb	0.34	0.39	0.24	0.26	0.3	0.33	0.36	0.26	0.22	0.39	0.46	0.54	0.56	0.84	0.27
Dy	2.24	2.68	1.8	1.43	1.94	1.93	2.23	1.35	1.23	2.72	2.39	2.8	2.86	3.84	1.75
Ho	0.44	0.58	0.42	0.29	0.4	0.36	0.5	0.31	0.25	0.62	0.42	0.49	0.44	0.68	0.38
Er	1.3	1.67	1.41	0.83	1.13	1.19	1.38	0.89	0.81	1.99	1.03	1.21	1.4	1.82	1.12

Continued

Tm	0.19	0.24	0.23	0.12	0.16	0.18	0.21	0.12	0.11	0.3	0.14	0.17	0.16	0.23	0.19
Yb	1.16	1.5	1.66	0.8	1.04	1.17	1.38	0.76	0.72	2.03	0.92	1.21	1.02	1.59	1.21
Lu	0.2	0.22	0.27	0.13	0.15	0.17	0.2	0.11	0.12	0.31	0.13	0.18	0.15	0.24	0.21
Mo	7	0.83	12.3	4.92	1.21	1	-	0.2	13	17.4	0.2	<0.1	0.1	1	3
Cu	2128.2	200.65	1100.27	46.2	411.69	9	38	101.3	1156.6	10066.16	37.9	10.7	7.1	40	1030
Pb	0.7	2.05	2.5	4.08	1.56	-	23	0.4	0.4	2.29	1	1.6	2.5		-
Zn	43	56.5	50.3	7.16	47.8	34	300	17	16	23.7	70	65	67	79	46
Ag	0.6	0.26	0.48	0.22	2.23	-	-	<0.1	0.2	2.62	<0.1	<0.1	<0.1		-
Ni	42	70.9	55.1	26.6	37.8	63	51	32.4	25.1	25.8	144.4	29.4	131.7	19	84
As	0.9	10.1	22.2	29	144.56	0.3	3.4	<0.5	1.2	11.1	3	1.9	1.7	1.1	3.4
Au	0.0812	0.8	0.16	0.21	0.498	-	-	0.0078	0.0273	0.38	0.002	0.0019	0.0029		
Cd	<0.1	-	-	-	-	-	-	<0.1	<0.1	-	<0.1	<0.1	<0.1		
Sb	1.6	10.2	5.11	49.9	5.65	0.05	0.06	0.8	1.2	13.8	0.7	0.8	1.3	0.18	0.39
Bi	<0.1	0.14	0.29	0.59	7.43	0.01	0.03	<0.1	<0.1	0.4	<0.1	<0.1	<0.1	0.51	0.12
Hg	0.04		-	-	-	0.173	0.045	<0.01	0.01	-	<0.01	<0.01	<0.01	0.022	0.037
Tl	<0.1	0.14	0.17	0.24	0.08	-	-	<0.1	<0.1	0.18	<0.1	<0.1	<0.1		-
Se	2.3	3.86	4.89	2.18	1.06	0.2	0.2	<0.5	<0.5	1.88	<0.5	<0.5	<0.5	0.2	1.3
Te	-	-	-	-	-	0.01	-	-	-	-	-	-	-	0.02	0.06
Cr	-	-	-	-	-	260	110	-	-	-	-	-	-		

Table 2. Suite of **Table 1**.

Sample	E27D	E23G	G5	G6	B2	G1	G3	B3	M2	D1	D2	E26D	E16G	E57G
Facies	Gabbro. microgabbro					Porphyry Diorite				Quartz Diorite quartzique		Dacite sphérolitique		
	Major elements (%)													
SiO_2	49.42	44.28	55.3	51.1	49.7	49.5	57.2	61.6	62.4	60.1	57.6	56.75	78.47	76.95
Al_2O_3	11.27	11.02	13.15	11.35	13.25	11.5	14.45	15.95	14	14.45	14.3	14.42	13	13.1
Fe_2O_3	18.93	16.51	9.4	10.8	15.3	8.33	8.33	7.72	6.34	9.77	6.82	7.13	1.17	1.29
CaO	5.89	7.61	6.84	7.14	9.57	6.7	4.16	3.01	5	2.11	5.09	7.09	0.56	0.59
MgO	3.84	5.09	5.64	9.66	6.38	5.83	3.9	3.19	2.97	2.25	3.47	2.31	0.36	0.35
Na_2O	3.14	1.66	2.41	2.24	1.72	0.76	2.75	4.13	4.34	3.47	4.02	1.12	1.55	3.26
K_2O	0.43	0	2.31	1.52	0.03	2.23	1.11	0.74	0.17	1.7	1.03	3.69	2.4	2.27
Cr_2O_3	0	0.009	0.03	0.06	0.01	0.06	0.02	0.01	0.02	0.02	0.03	0.015	0	0
TiO_2	2.05	2.16	0.63	0.56	0.81	0.42	0.48	0.43	0.33	0.39	0.45	0.38	0.04	0.04
MnO	0.07	0.32	0.16	0.14	0.22	0.08	0.06	0.04	0.05	0.01	0.05	0.04	0.02	0.04
P_2O_5	0.2	0.17	0.23	0.21	0.07	0.1	0.11	0.12	0.06	0.07	0.08	0.07	0.03	0.02
LOI	4.4	11	2	2.78	2.67	12.7	6.77	3.04	2	2.8	2.28	6.8	2.3	2

Continued

Traces elements (ppm)														
Ni	32	70	-	-	-	-	-	-	-	-	-	36	<20	<20
Sc	39	28	-	-	-	-	-	-	-	-	-	15	2	3
Ba	49	25	621	1235	11.1	272	189.5	194	97.1	208	150.5	204	250	192
Be	<1	2	-	-	-	-	-	-	-	-	-	<1	1	<1
Co	30.1	27.7	65	52	54.9	28	30	16.3	90	108	64	16.3	0.5	1
Cs	1.1	0.3	1.01	1.64	0.25	1.81	1.07	0.42	0.16	1.35	1.41	7.2	4	2.7
Ga	15.7	18	14.9	12.1	14.6	14.4	17.1	17.3	14.9	20.2	16.6	14.1	12.8	13.2
Hf	3.5	3.1	1.4	1.6	1.4	1.5	2	2.1	1.9	2.2	2.3	1.8	2	2
Nb	5.1	7.9	4.9	3.4	0.9	3.6	4	3.1	2.1	3.2	2.9	1.5	5.5	6.5
Rb	17.5	0.4	72.4	39.1	0.4	66.7	31.7	20.9	4.3	65.1	39.7	142.9	59.7	61.5
Sn	2	3	1	1	-	1	1	-	1	1	1	<1	1	1
Sr	127.8	109.9	324	139.5	131.5	78.1	120.5	379	441	253	388	69.8	96.5	35.4
Ta	0.3	0.5	0.2	0.3	-	0.2	0.3	0.2	0.2	0.3	0.2	<0.1	1	0.9
Th	0.6	0.8	0.76	0.95	0.08	0.81	0.92	0.97	0.77	1	0.8	0.8	2.7	2.5
U	0.9	0.3	0.34	0.71	<0.05	0.4	0.65	0.23	0.31	0.4	0.47	0.4	1.7	2
V	437	350	213	217	309	130	146	124	92	123	120	108	<8	<8
W	2.5	2.6	224	69	-	19	26	1	367	247	253	1.5	1.1	<0.5
Zr	129.3	116.7	46	61	40	52	71	69	70	73	78	62.1	39.7	45.9
Y	43.9	21.5	16	15.7	23.8	10.2	12.2	10.1	7.9	3.8	11.2	6.5	11.8	10.8
La	8	9.8	9.4	8.2	1.2	11.1	5.9	6.1	5.4	4.1	6.3	4.2	7.8	7.7
Ce	21.8	24.5	19.3	18.1	3.8	21.9	12.5	12.6	12.7	8.5	14.7	9.8	14.6	17
Pr	3.24	3.63	2.62	2.38	0.69	2.71	1.63	1.8	1.71	1.03	2.06	1.38	1.69	1.84
Nd	14.4	16.8	11.1	10.4	4.1	10.5	7.1	8.1	7.5	4.4	9.1	6.3	6.2	6.4
Sm	4.79	4.37	2.67	2.72	1.55	2.16	1.79	1.87	1.73	0.92	2.23	1.48	1.58	1.46
Eu	1.42	1.57	0.92	0.9	0.76	0.64	0.53	0.66	0.54	0.43	0.68	0.41	0.2	0.16
Gd	5.8	4.47	2.92	2.62	2.62	2.11	2.04	1.94	1.62	0.87	2.23	1.32	1.63	1.57
Tb	1.11	0.77	0.49	0.44	0.53	0.35	0.36	0.29	0.24	0.12	0.35	0.21	0.34	0.3
Dy	7.29	4.49	2.88	2.69	4	1.93	2.22	1.79	1.46	0.66	2.05	1.22	1.97	2.02
Ho	1.63	0.83	0.58	0.5	0.89	0.39	0.45	0.37	0.3	0.14	0.43	0.25	0.39	0.37
Er	4.84	2.2	1.64	1.64	2.72	1.11	1.32	1.06	0.9	0.4	1.28	0.74	1.06	0.99
Tm	0.71	0.3	0.23	0.25	0.43	0.16	0.19	0.17	0.12	0.06	0.18	0.12	0.14	0.16
Yb	4.85	2.06	1.58	1.68	2.59	1.19	1.41	1.07	0.85	0.38	1.23	0.75	0.98	1.04
Lu	0.77	0.29	0.25	0.25	0.42	0.18	0.22	0.17	0.14	0.06	0.2	0.14	0.13	0.15
Mo	1.2	0.3	1	2	-	1	1	-	1	1	1	0.5	<0.1	0.2
Cu	1012.9	71.8	104	1960	161	753	1305	1620	204	868	160	388.8	4.3	3.6
Pb	1	0.5	-	-	-	-	-	-	-	-	-	0.4	1.5	1.4

Continued

Zn	33	59	116	68	98	25	31	24	20	18	30	20	11	8
Ag	0.3	<0.1	-	-	-	-	-	-	-	-	-	<0.1	<0.1	<0.1
Ni	31.5	66.8	31	61	53	76	54	38	32	28	44	31	1.4	1.1
As	1.1	1.7	0.7	0.5	0.8	0.6	0.6	0.7	1	0.6	0.5	0.7	4.1	3.3
Au*	0.033.9	0.004.9	-	-	-	-	-	-	-	-	-	0.0279	0.0072	0.0007
Cd	<0.1	<0.1	-	-	-	-	-	-	-	-	-	<0.1	<0.1	<0.1
Sb	1.1	0.9	0.05	0.05	0.17	0.17	0.11	0.12	0.05	0.09	0.12	0.6	0.7	0.5
Bi	0.3	<0.1	0.02	0.54	0.01	0.03	0.08	-	0.01	0.86	0.03	0.1	<0.1	<0.1
Hg	0.01	<0.01	0.14	0.074	0.011	0.02	0.048	0.012	0.3	0.212	0.215	<0.01	0.1	0.02
Tl	<0.1	<0.1	-	-	-	-	-	-	-	-	-	<0.1	<0.1	<0.1
Se	0.6	<0.5	0.2	0.3	0.5	0.6	2	-	0.2	0.6	0.2	<0.5	<0.5	<0.5
Te	-	-	0.01	0.04	0.04	0.02	0.06	0.02	0.01	0.07	0.01	-	-	-
Cr	-	-	250	480	40	440	160	90	200	150	170	-	-	-

In the two laboratories, major elements were analyzed by inductively coupled plasma-atomic emission spectrometry (ICP-AES), whereas traces elements data were obtained by inductively coupled plasma mass spectrometry (ICP-MS).

These data were supplemented by thirteen whole rock analyses results from [27] and [42] studies in the study area. All of these samples were analyzed in ALS Chemex laboratories in Spain and Canada by ICP-AES for major elements and ICP-MS for trace elements.

3.4. Sulfur Isotopic Analysis

Four rock samples containing pyrite and chalcopyrite were sent to Actlabs in Vancouver (Canada) for extraction and analyses. Dried samples are weighted into tin cups for 34S analysis. Approximately 0.3 mg of sample is used for 34S analysis, with 3 mg of niobium pentoxide added to each sample to ensure complete sample combustion. Samples are loaded into a Fisons Instruments elemental to be flash combusted at 980° C. Released gases are carried by ultrapure helium through the analyzer, then separated by gas chromatography. Clean SO2 gas is carried into the Mat 253, Thermo Scientific, IRMS for analysis. Data is corrected and normalized using three international standards, IAEA SO6, IAEA SO5, NBS 127, and two calibrated internal standards that bracket the samples. Standards are at the beginning and end of every run. The δ34S values are reported relative to the Vienna Cañon Diablo Troilite (VCDT) standard.

3.5. Microprobes Analysis

Microprobe analyses by CAMECA SX100 were carried out at the "Magmas et Volcan" Laboratory of the Clermont-Ferrand University (France). They involved a total of four core samples from the study area. These analyses aim to determine

the different mineral phases of these rocks in order to determine their petrogenetic characteristics and their paragenetic sequence. Epidotes, chlorites, feldspars, carbonates and amphiboles are the hydrothermal alteration minerals which have been analyzed.

3.6. Correlation Factor Analyses

Preliminary factor analyses were conducted to define factors related to hydrothermal alteration and mineralization using SPSS 16.0 software to analyze eleven rock samples. The trace elements used for this analysis are copper (Cu), gold (Au), silver (Ag), molybdenum (Mo), selenium (Se), antimony (Sb), nickel (Ni), lead (Pb), zinc (Zn), mercury (Hg), barium (Ba), arsenic (as), strontium (Sr), rubidium (Rb), cesium (Cs), bismuth (Bi). The major elements are represented by Fe_2O_3, TiO_2, loss on ignition (LOI), total carbon (TOT/C) and total sulfur (TOT/S). Alteration indexes were also used. These are those of [45] (AI, SI), [46] (CCPI) and [47] (IP or potential index). The AI generally indicates chlorite-sericite alteration, the CCPI indicates chlorite-carbonate-pyrite alteration and SI indicates the silicification index.

4. Results

4.1. Hydrothermal Alteration Minerals

Hydrothermal alteration is an important factor in the genesis of hydrothermal deposits in magmatic and metamorphic contexts. In the Gongondy and Diénéméra deposits, several types of alteration have been identified on the basis of petrographic observations.

4.1.1. Sericitic Alteration

Sericitic alteration affected spherulitic dacite (Gongondy) and, to a lesser extent, Quartz porphyry microdiorite (Diénéméra) (**Figure 3(A)**). This alteration is marked by abundant sericite associated with secondary quartz, carbonates and chlorite in minute quantities, accompanied by deposition of abundant metallic opaque crystals, either in fine disseminations or fractured coarse-grains, cemented by quartz and carbonates. Sericite occurs in fine lamellae (40 wt% - 50 wt%), resulting from partial or total destruction of the feldspars. In facies affected by these types of alteration, sericite is also found in the form of veinlets deposited around other veinlets, particularly early quartz-carbonate veinlets. Greenish chlorite is present in small quantities (5 wt% - 15wt%). It is practically associated with disseminated sulfides, which represent around 15-20wt% of the rock minerals (**Figure 4(A)**).

In dacite and Quartz porphyry microdiorite, a second type of sericite alteration occurs late or coexists with the first. This latter type of alteration is dominated by white micas (50 wt% - 55 wt%) associated with accessory carbonates (5 wt% - 10 wt%). Rocks affected by these types of alteration take on a light green or yellowish color (**Figure 3(B)**). This type of hydrothermal alteration can also be found in

fractures or veinlets (Figure 3(C)). Micas occur in more or less oriented lamellae. Sulfides (5wt%) are rare, fine (80 μm) and automorphs, disseminated in the rock, moulded by phyllites consisting mainly of white mica (Figure 4(B)).

4.1.2. Propylitic Alteration

Propylitic alteration affects quartz porphyry microdiorite, spherulitic microdiorite, intersertal microdiorite and quartz diorite. At a macroscopic scale, altered rocks take on a light green color (Figure 3(D)). At a microscopic scale, it is characterized by an epidote-chlorite-sericite assemblage, with varying content of carbonates, quartz and albite (Figure 4(C)). Epidote (15 wt% - 45 wt%) is the result of the destabilization of plagioclases and amphiboles. Chlorite (10 wt% - 35 wt%) is largely derived from ferromagnesian minerals (biotite, amphibole) and plagioclases, which are also altered into sericite. Carbonates come from the decomposition of feldspars and amphibole. Slight albitization (5 wt% - 10 wt%) related to saussuritisation of the plagioclases is associated with propylitic alteration in these intermediate rocks (Figure 4(H)).

4.1.3. Phyllitic-Carbonate Alteration

The Phyllitic-carbonate alteration is marked by the predominance of phyllites (chlorite and sericite) (50 wt% - 60 wt%) over carbonates (15 wt% - 20 wt%) and, conversely, by the predominance of carbonates (55 wt% - 60 wt%) over phyllites (30 wt% - 35wt%) for the carbonate-phyllitic type. At Gongondy, where these types of alteration are most pronounced, a certain zonation is observed according to the dominance of one of the three phases. Chlorite dominates at the surface, sericite in the intermediate part and carbonates at deeper zones. Depending on the dominance of a particular mineral, the rock can take on a white, grey or light green color (Figure 3(E)). Sericite (15 wt% - 35 wt%) comes mainly from the partial destabilization of feldspars and is present in fine flakes. Chlorite (10 wt% - 25 wt%) results mainly from the alteration of ferromagnesian minerals (amphiboles, biotite) or, to a lesser extent, feldspars. Carbonates (10 wt% - 60 wt%) come from the destabilization of feldspar or ferromagnesian minerals (amphibole, biotite) (Figure 4(D)).

4.1.4. Chloritic Alteration

Chloritic alteration affects microdiorite porphyry and microgabbro (Figure 3(F)). Microscopically, massive chlorite alteration (40 wt% - 60 wt%) almost completely invades the rocks in question and is associated with sericite (10 wt% - 15 wt%), carbonates (10 wt% - 15 wt%) and quartz (10 wt%). Accessory elements (10 wt%) are represented by opaques (pyrite, rutile, etc.). This chlorite can be distinguished from that observed in the mineralized zones by its bluish hue, suggesting a different composition. Chlorite is the product of the destabilization of feldspar or ferromagnesian minerals (amphibole, biotite) (Figure 4(E)).

4.1.5. Potassic Alteration

Traces of potassic alteration were observed in borehole S16G at Gongondy. It af-

fects a pinkish microgabbro-diorite dyke injected into an ophitic microdiorite. Microscopic evidence of this alteration shows the transformation of amphibole to biotite and the perthitisation of plagioclase (Figure 4(F)). This type of alteration is also suspected in a late intrusion of microdiorite porphyry, which shows a similar reddish color.

4.1.6. Silicification

Silicification of rocks is common in the study area. The alteration is frequently visible in the Diénéméra deposit. It is characterized by quartz veins and veinlets, or silica partially or completely invading quartz microdiorite porphyries, spherulitic microgabbros, microgranodiorites and microgranites. Microscopically, silicification leads to the formation of ribbons of quartz, often polygonal, associated with coarse carbonate and opaque crystals (Figure 4(G)). It also appears in the form of coarse quartz veinlets in quartz microdiorites. It forms the cement for the coarse cracked pyrite crystals.

Figure 3. Macroscopic view of altered rocks from Diénéméra-Gongondy copper deposits. Sericitic alteration 1 affecting microdiorite porphyry at Gongondy (A). Sericite alteration 2 affecting dacitic rocks: Pervasive alteration (B) and alteration saw in veinlet (C). Propylitic alteration affecting Quartz porphyry microdiorite in Diénéméra (D). Phyllito-carbonate alteration affecting microdiorite in Gongondy deposit (E). Chloritic alteration affecting porphyry microdiorite in Gongondy (F).

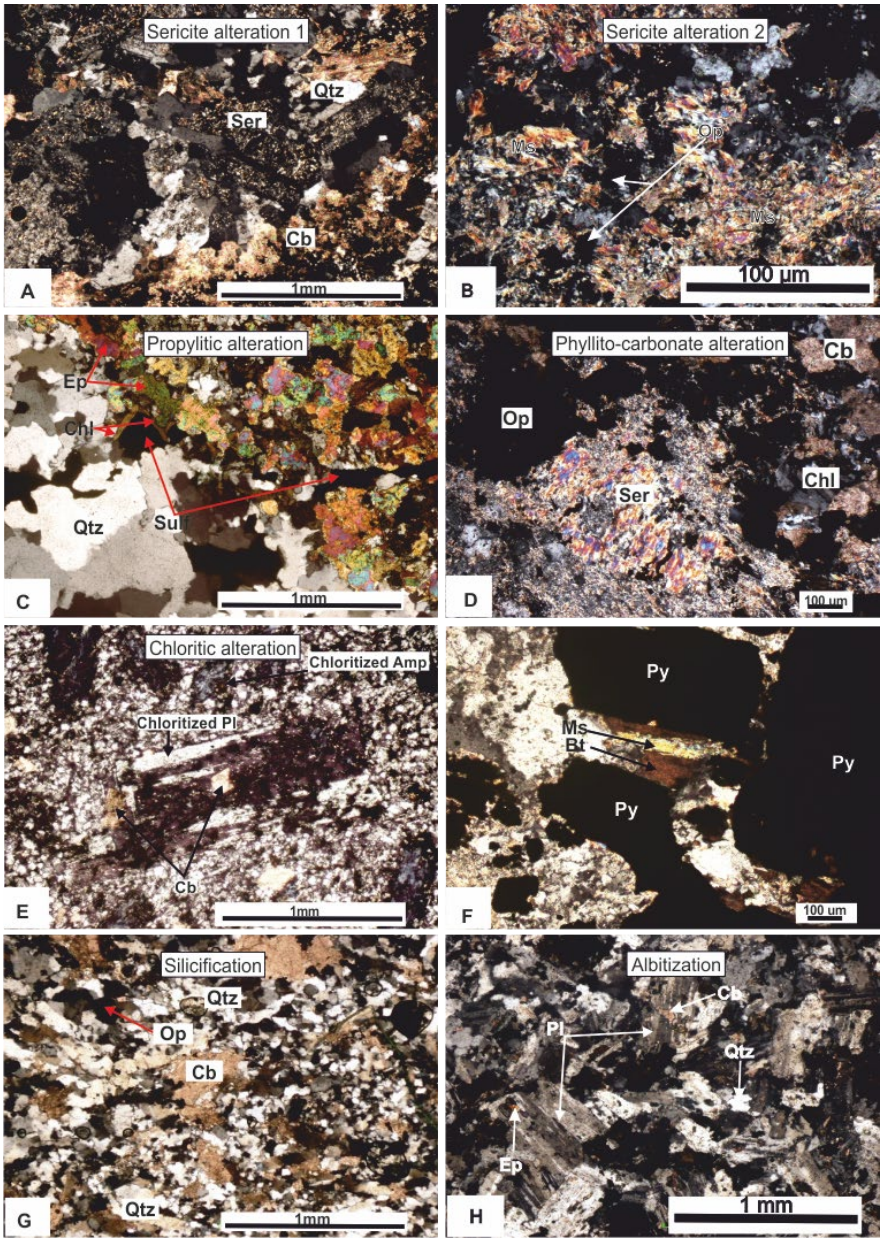

Figure 4. Microscopic view of altered rocks from Diénéméra-Gongondy copper deposits. Sericitic alteration 1 (A), Sericitic alteration 2 (B), Propylitic alteration (C), Phyllitic-carbonate alteration (D), Chloritic alteration (E), Residual potassic alteration (F), Silicification (G) and Albitization (H). Minerals abbreviations: Amp: Amphibole, Bt: biotite, Cb: carbonate, Chl: chlorite, Ep: epidote, Ms: muscovite, Op: Opaques; Pl: plagioclase; Py: pyrite, Qtz: quartz, Ser: sericite, Sulf: sulfides.

Finally, silicification is associated with shearing in the form of centimetric to decimetric quartz veins.

4.2. Geochemistry of Hydrothermal Alteration

Macroscopic and microscopic studies of hydrothermal alteration in the study area show that all samples are subject of hydrothermal alteration. Based on the altera-

tion mineral assemblages, several patterns of hydrothermal alterations have been defined. The geochemical analysis of major and trace elements can be used to define the mobility of some elements such as K_2O, Na_2O. The binary diagram of [48] modified by [49] discriminated less altered rocks from the very altered ones (**Figure 5**).

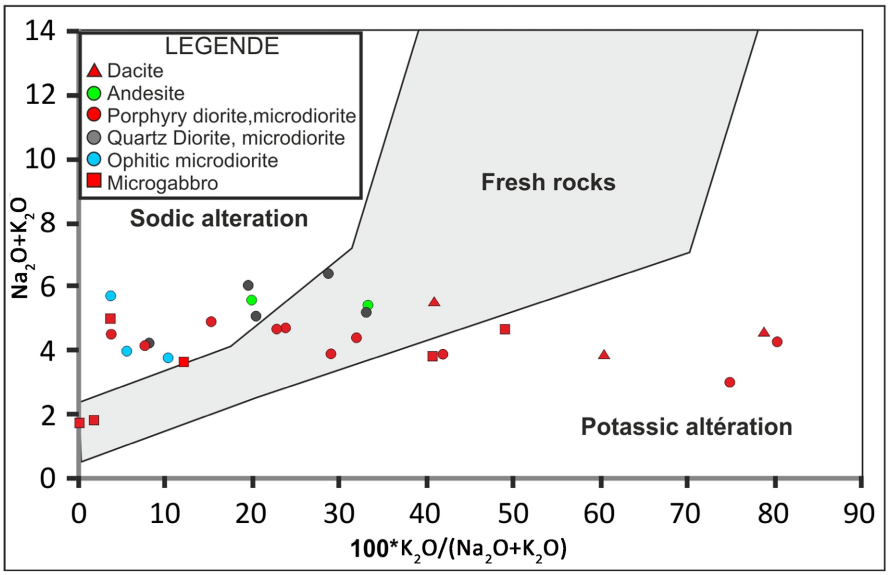

Figure 5. Binary diagram of [48] modified by [49] discriminating the fresh rocks to altered rocks.

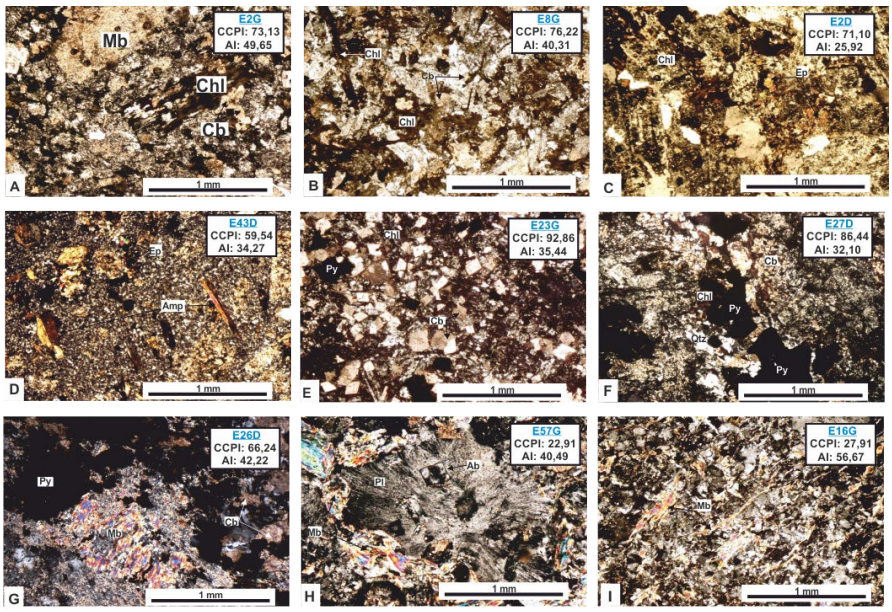

Figure 6. CCPI and AI for different types of alteration observed in the study zone. Phyllitic-carbonate alteration (A) (B), Propylitic alteration (C) (D), chloritic alteration (E) (F), Sericite alteration 1 (I), Sericite alteration 2 (G) (H).

Most of the samples analyzed are altered, but the degree of alteration varies.

The ophitic rocks are characterized by an exclusive sodic alteration. The alteration indexes of [45] and [46] have been important to distinguish the different types of hydrothermal alteration. Propylitized rocks according to petrographic observations show a low CCPI (60 to 75) and medium AI (25 to 35) (**Figure 6(C)** and **Figure 6(D)**) whereas phyllitic-carbonate altered rocks show a relatively high CCPI (75 to 85) and AI (50 to 60) (**Figure 6(A)** and **Figure 6(B)**). These two types of alteration are clearly distinguishable from sericitic and chloritic alteration, which have higher AI and CCPI values respectively. Chloritic alteration in relation with mafic rocks has a low AI like propylitic alteration, with high CCPI between 85 and 100 (**Figure 6(E)** and **Figure 6(F)**). Sericite alteration 1, on the other hand, shows an AI (50 to 70) that is similar to that of phyllitic-carbonate alteration, for a low CCPI between 20 to 30 (**Figure 6(G)**). Sericitic alteration 2 differs from the sericitic alteration 1 by a lower value of CCPI which is less than 30 (**Figure 6(H)** and **Figure 6(I)**).

In the ternary diagram of [50], an evidence of sericitization is observed in all rocks with a tendency for chloritization, notably for mafic rocks (**Figure 7(A)**). However, the diagram of [51] shows a clear segregation of rocks in different alteration fields. Dacitic rocks fall in the sericitic and propylitic fields. Gabbroic rocks are generally observed in the propylitic field only. Intermediate rocks are observed in the propylitic fields dominantly quartz microdiorite porphyry, quartz diorite porphyry, and ophitic microdiorites. Porphyric microdiorites, porphyric diorites and andesites are observed in the K-silicate fields in relation with K-Feldspar alteration (**Figure 7(B)**).

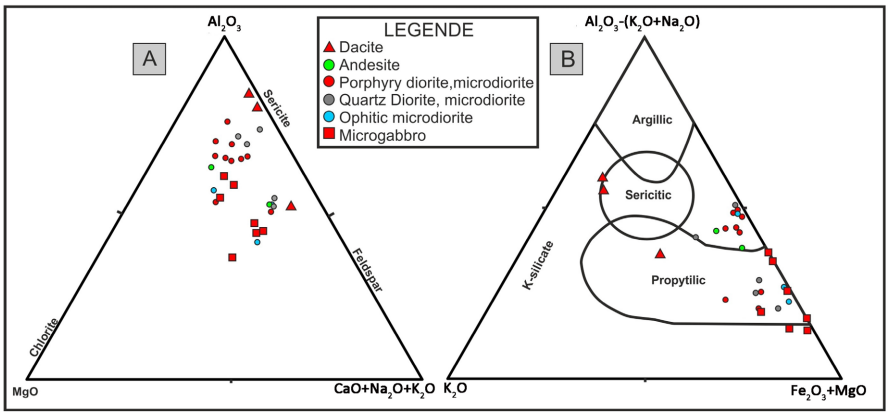

Figure 7. Hydrothermal alteration diagram using major elements. Ternary diagrams of [50] (A) and [51] (B) which define some fields of hydrothermal alterations.

4.3. Alteration Mineral Chemistry

The chemical analyses of some minerals which are frequent in the alteration zone of Diénéméra-Gongondy porphyry copper (plagioclase, chlorite, epidote, amphibole, carbonate) enabled us to define the chemical composition of these minerals and the consequently determine the type of fluid responsible for the alteration and the deposition of the mineralization. The details of chemical analyses of minerals are found in **Table 3** and **Table 4**.

4.3.1. Plagioclase

Four samples were used to study the chemical composition of the plagioclase found in the study area. All analyzed points show a high proportion of SiO_2 (66.43 wt% - 71.69 wt%), Al_2O_3 (18.08 wt% - 20.27 wt%), Na_2O (8.81 wt% - 10.91 wt%) and a low proportion of K_2O (0.006 wt% - 0.31 wt%) and CaO (0.07 wt% - 0.60 wt%). The percentage of K and Ca are less than 1 wt%, whereas the proportion of Na is higher, varying between 3.08 and 3.66 wt%. According to the ternary Ab-An-Or diagram of [52] for the classification of plagioclase, all the samples analyzed fall in the albite field (**Figure 8(A)**).

4.3.2. Epidote

Five points of epidotes were analyzed. These epidotes have a homogeneous chemical composition, with higher content of Al_2O_3 than FeOt and Cr_2O_3. Moreover, the content of CaO is high, ranging from 22.87 to 23.77 wt%. The Al_2O_3 content shows very little variation between 21.77 and 22.90 wt%. Total iron content range from 12.82 and 13.82 wt%, whereas the content of chromium is below than 0.1%. The Al-Cr-Fe ternary diagram of [53] shows that the epidotes have a composition of clinozoisite (**Figure 8(B)**).

4.3.3. Carbonate

Carbonate are fairly ubiquitous in the Diénéméra and Gongondy deposits. Seven carbonates points from three rock samples were analyzed chemically. A wide variation in CaO (28.99 wt% - 58.29 wt%), MgO (0.02 wt% - 9.45 wt%) and FeOt (0.10 wt% - 13.98 wt%) was observed depending on the type of carbonate present in the rocks. The carbonate of sample E11G is distinguished from the other carbonates by high MgO and FeOt contents (9.45 wt.% and 13.98 wt.%, respectively and a correspondingly lower CaO content (28.99 wt%). The Mg-Ca-Fe ternary diagram of [54] shows that all carbonates have a composition close to calcite, except the carbonates of sample E11G, which lies between dolomite and ankerite composition (**Figure 8(C)**). In the Mg-Fe-Mn diagram of [54], the carbonate of sample E11G falls in the field of Fe-dolomite (**Figure 8(D)**).

4.3.4. Chlorite

Chlorite is an abundant mineral in the rocks in the study area. The chemical composition of the mineral shows a high proportion of SiO_2 (23.83 wt% - 29.78 wt%), Al_2O_3 (13.18 wt% - 23.30 wt%) and low proportions of CaO (0 wt% - 0.38 wt%), K_2O (0 wt% - 0.82 wt%) and Na_2O (< 0.20 wt%). The proportions of MgO (9.12 wt% - 20.01 wt%) and FeOt (18.03 wt% - 33.03 wt%) vary depending to the samples. The lowest proportions of MgO are found in the chlorite of samples E22G where this proportion of of FeOt (31.04 wt% - 33.03 wt%) than other chlorites. Other samples have a relatively same proportion of FeOt and MgO. The content of TiO_2 of most samples is less than 0.1% except for samples E11G where the content is more than 0.4%. In binary diagram of [55], the chlorites from sample E22G fall into the ripidolite field. whereas the chlorites from the other samples are of types of ripidolite and pycnochlorite fields (**Figure 8(E)**).

4.3.5. Amphibole

The chemical composition of 3 amphiboles points was analyzed. The contents of SiO_2 (52.93 - 54.89 wt%), FeOt (9.07 wt% - 11.32 wt%), MgO (16.63 wt% - 18.01 wt%) and CaO (11.58 wt% - 12.28 wt%) are high. Low contents are observed for TiO_2 (0.25 wt% - 0.27 wt%), Na_2O (0.46 wt% -0.52 wt%) and K_2O (0.03 wt% - 0.11 wt%). The diagram of [56] also shows two different sources of amphiboles: primary and secondary (**Figure 8(F)**). The diagram of [57] shows that amphiboles are from two types: actinolite and magnesio-hornblende (**Figure 8(G)**).

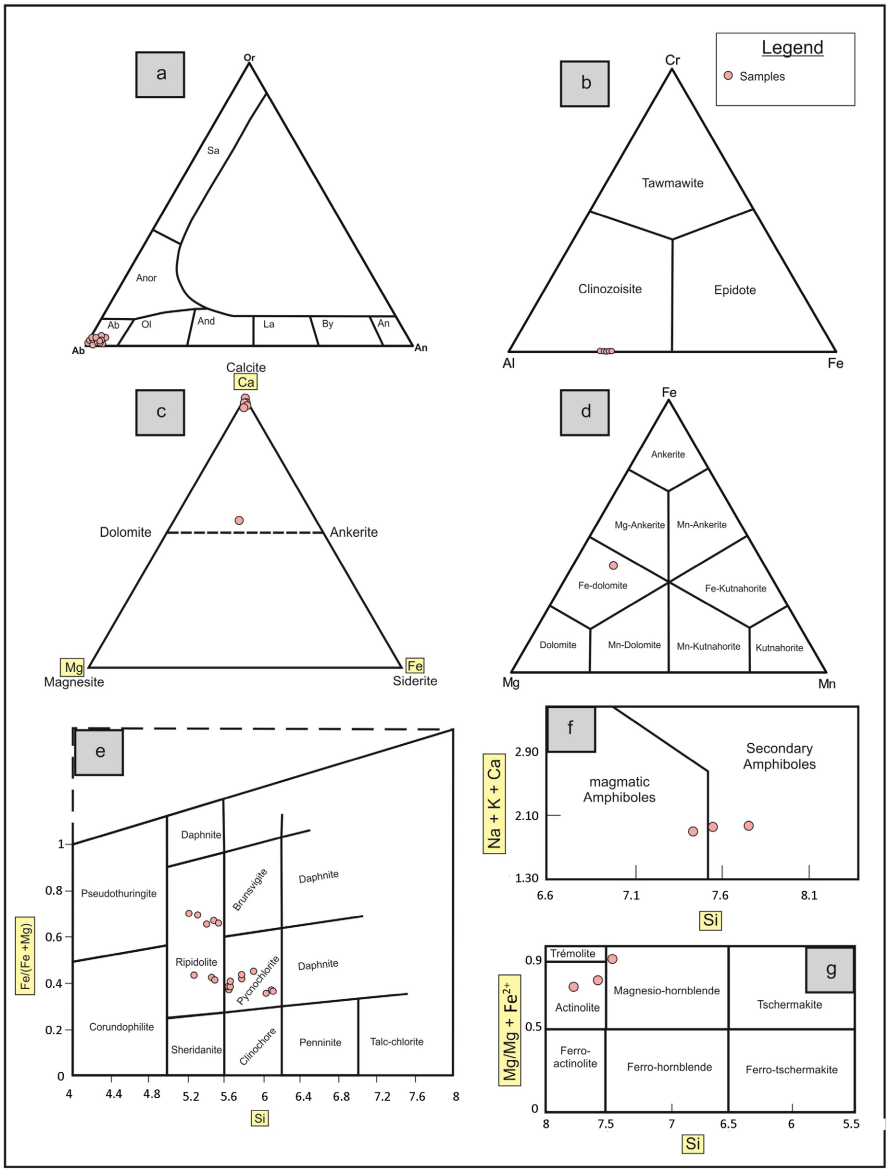

Figure 8. Diagrams of alteration minerals chemistry. Ab-An-Or ternary diagram for classifying plagioclase [52] (A). Al-Cr-Fe ternary diagram for epidote classification [53] (B). The Mg-Ca-Fe ternary diagram of carbonates classification [54] (C). the Mg-Fe-Mn diagram of [54] is used to discriminate Fe-carbonates (D). Binary diagram of chlorite classification [55] showing two groups of chlorites (E). Classification binary diagram of amphibole according to the origin [56] (F) and the composition [57] (G).

Table 3. Chemical composition of minerals: major elements.

	Comment	DataSet/Point	SiO_2	TiO_2	Al_2O_3	Cr_2O_3	FeOt	MnO	MgO	CaO	Na_2O	K_2O	Total
	Lame 21D	12	68.6392	0	19.843	0.002	0.0224	0	0	0.2717	10.6663	0.0878	99.5325
	Lame E7D	19	68.7006	0.0269	20.0332	0	0.1106	0	0	0.3115	10.7833	0.0632	100.0293
	Lame E7D	20	66.4361	0.0077	19.519	0.026	0.5513	0	0.0789	0.5149	8.8177	0.1926	96.1442
	Lame E7D	21	71.6964	0.0115	18.0874	0.024	0.0914	0	0	0.0732	9.9697	0.0062	99.9597
	Lame E7D	22	70.2831	0	19.5659	0	0.0834	0.0131	0	0.105	10.5183	0.0586	100.6274
	Lame E7D	27	68.9615	0	19.8569	0.012	0	0.0185	0.0228	0.3672	10.8533	0.0663	100.1585
Plagioclase	Lame E7D	29	68.3212	0	20.1293	0.03	0.0834	0.0361	0	0.6009	10.8576	0.0416	100.1002
	Lame E7D	31	69.1764	0.0268	19.8246	0.0334	0.0878	0.0019	0	0.2242	11.0196	0.0487	100.4432
	Lame E7D	34	69.4997	0	20.0036	0.013	0.1621	0.0188	0	0.1135	10.9474	0.03	100.7882
	Lame E11G	54	68.9643	0.0214	20.0251	0.0112	0.243	0.0103	0.0034	0.4169	10.8048	0.0358	100.5363
	Lame E11G	61	68.8879	0.025	19.884	0.006	0.5037	0	0.0083	0.1527	10.82	0.1389	100.4264
	Lame E11G	62	69.5917	0.0374	20.1589	0	0.4479	0	0	0.1446	10.9138	0.073	101.3673
	Lame E11G	68	68.8152	0.02	20.1057	0.0057	0.1548	0	0	0.2047	10.313	0.0701	99.6893
	Lame E11G	69	68.1315	0	20.2778	0.0111	0.1459	0	0.0356	0.3958	10.3469	0.3178	99.6625
	Comment	DataSet/Point	SiO_2	TiO_2	Al_2O_3	Cr_2O_3	FeOt	MnO	MgO	CaO	Na_2O	K_2O	Total
	Lame 21D	3	26.7559	0.018	17.8873	0	22.7905	0.1526	16.8718	0.0605	0.0644	0.1278	84.7288
	Lame 21D	4	27.3031	0.0879	16.918	0.1701	23.4087	0.2668	16.0471	0.3859	0.0721	0.1245	84.7842
	Lame 21D	10	27.5321	0.0154	18.4637	0.0546	22.648	0.1584	17.6807	0.0717	0.0115	0	86.6361
	Lame 21D	11	26.9206	0.0325	19.3256	0.0415	21.9077	0.2012	17.8353	0	0.0137	0	86.2782
	Lame E7D	17	27.2573	0.0235	20.3247	0.0289	20.9802	0.0545	18.1994	0.0151	0	0.0368	86.9204
	Lame E7D	18	29.7875	0.1959	19.563	0.0387	18.0352	0.0681	17.38	0.0613	0.0083	0.8187	85.9566
	Lame E7D	23	27.2877	0.0381	20.2588	0.0528	20.7564	0.0632	18.2829	0.0183	0.0085	0	86.7668
	Lame E7D	24	25.9168	0.0235	20.8782	0.0362	22.1446	0.0952	17.1202	0.0015	0.0276	0.0517	86.2955
Chlorite	Lame E7D	32	25.0515	0.0352	22.4787	0	22.3364	0.0584	16.4831	0.0352	0.0048	0.0151	86.4984
	Lame E7D	33	26.3539	0	21.1799	0.0054	21.661	0.0979	17.4595	0	0.0086	0.0148	86.781
	Lame E7D	35	27.3277	0.0405	20.2749	0.0017	20.9877	0.0869	18.4431	0.0411	0.0111	0.0151	87.2297
	Lame E22G	44	23.8325	0.0326	22.3008	0	32.9933	0.1935	8.8575	0.0207	0.0053	0.0188	88.255
	Lame E22G	45	24.4881	0	21.8799	0.0277	33.0363	0.2646	9.1207	0	0.0495	0	88.8669
	Lame E22G	50	25.7404	0.0396	21.4751	0.0504	31.0484	0.1338	9.8946	0.0306	0.0035	0.042	88.4582
	Lame E22G	51	26.1132	0.0593	23.3057	0.0439	31.4272	0.152	10.1769	0.0765	0.1092	0.0758	91.5398
	Lame E22G	52	25.9103	0.023	22.2617	0.0437	31.621	0.2297	9.6233	0.0846	0.0418	0.0864	89.9255
	Lame E11G	66	29.0185	0.5128	16.1821	0.0238	20.0301	0.1808	18.94	0.2012	0.0047	0.1776	85.2717
	Lame E11G	67	29.1443	0.4152	16.3992	0.0085	19.9778	0.1898	20.0158	0.1689	0.0142	0.0924	86.4259
	Comment	DataSet/Point	SiO_2	TiO_2	Al_2O_3	Cr_2O_3	FeOt	MnO	MgO	CaO	Na_2O	K_2O	Total
Carbonate	Lame 21D	1	0.0267	0.0258	0.0016	0	0.1023	0.0938	0.0259	57.883	0.0162	0	58.1753
	Lame E22G	41	0.2343	0.0455	0.0715	0	1.3306	1.7933	0.3345	58.2378	0.0148	0.022	62.0842

Continued

	Lame E22G	42	0.0098	0	0.0112	0	1.5568	1.9313	0.4058	58.2958	0.0204	0.0313	62.2623
	Lame E22G	43	0.0007	0	0.0037	0	1.209	1.5275	0.294	56.9121	0.0068	0.0204	59.9743
	Lame E22G	48	0.0007	0.0349	0.0333	0	1.3335	1.8355	0.2802	57.0587	0	0.014	60.5908
	Lame E22G	49	0.0203	0	0	0	1.5601	2.0087	0.4221	58.0076	0.0017	0	62.0207
	Lame E11G	55	0.0769	0	0	0	13.9849	4.4293	9.4537	28.9905	0.0262	0.0131	56.9747
Epidote	Comment	DataSet/Point	SiO_2	TiO_2	Al_2O_3	Cr_2O_3	FeOt	MnO	MgO	CaO	Na_2O	K_2O	Total
	Lame E11G	56	37.9187	0.1253	22.902	0	12.8212	0.1168	0.0294	23.2458	0.0126	0.012	97.1837
	Lame E11G	57	37.8813	0.0617	22.5317	0	13.1418	0.1075	0.0116	23.7781	0	0	97.5138
	Lame E11G	58	37.9829	0.1269	22.102	0.0305	13.2017	0.0707	0	22.8727	0.0412	0	96.4286
	Lame E11G	59	37.7682	0.0704	21.7742	0.0322	13.7735	0.0645	0	23.3699	0	0.0173	96.8702
	Lame E11G	70	37.7488	0.1596	21.7731	0.0107	13.8206	0.078	0	23.1251	0.0254	0	96.7413
Amphibole	Comment	DataSet/Point	SiO_2	TiO_2	Al_2O_3	Cr_2O_3	FeOt	MnO	MgO	CaO	Na_2O	K_2O	Total
	Lame E11G	60	54.8996	0.2691	2.0425	0	9.0754	0.1828	18.0143	12.2873	0.4672	0.0363	97.2747
	Lame E11G	63	52.9398	0.2506	3.4974	0.0199	9.7912	0.2624	17.9715	11.4933	0.4922	0.1157	96.834
	Lame E11G	64	53.0791	0.3604	3.325	0.0411	11.3188	0.2027	16.636	11.5877	0.5195	0.0861	97.1565

Table 4. Chemical composition of minerals: trace elements.

Plagioclase	Si	Ti	Al	Cr	Fe	Mn	Mg	Ca	Na	K	**Total**
	11.998	-	4.088	-	0.003	-	-	0.051	3.615	0.020	19.775
	11.962	0.004	4.111	-	0.016	-	-	0.058	3.640	0.014	19.806
	11.996	0.001	4.154	0.004	0.083	-	0.021	0.100	3.087	0.044	19.490
	12.386	0.001	3.683	0.003	0.013	-	-	0.014	3.339	0.001	19.440
	12.119	-	3.976	-	0.012	0.002	-	0.019	3.516	0.013	19.658
	11.990	-	4.069	0.002	-	0.003	0.006	0.068	3.659	0.015	19.811
	11.910	-	4.136	0.004	0.012	0.005	-	0.112	3.670	0.009	19.859
	11.997	0.003	4.052	0.005	0.013	-	-	0.042	3.705	0.011	19.829
	12.003	-	4.072	0.002	0.023	0.003	-	0.021	3.666	0.007	19.796
	11.959	0.003	4.093	0.002	0.035	0.002	0.001	0.077	3.633	0.008	19.812
	11.971	0.003	4.072	0.001	0.073	-	0.002	0.028	3.646	0.031	19.827
	11.971	0.005	4.087	-	0.064	-	-	0.027	3.640	0.016	19.809
	11.994	0.003	4.130	0.001	0.023	-	-	0.038	3.485	0.016	19.689
	11.917	-	4.180	0.002	0.021	-	0.009	0.074	3.509	0.071	19.783
Chlorite	Si	Ti	Al	Cr	Fe	Mn	Mg	Ca	Na	K	**Si + Al**
28 oxygènes	5.776	0.003	4.551	-	4.114	0.028	5.429	0.014	0.027	0.035	8.000
	5.920	0.014	4.323	0.029	4.245	0.049	5.187	0.090	0.030	0.034	8.000
	5.783	0.002	4.570	0.009	3.978	0.028	5.536	0.016	0.005	-	8.000
	5.659	0.005	4.788	0.007	3.851	0.036	5.589	-	0.006	-	8.000

Continued

	5.642	0.004	4.958	0.005	3.632	0.010	5.616	0.003	-	0.010	8.000
	6.126	0.030	4.742	0.006	3.102	0.012	5.329	0.014	0.003	0.215	8.000
	5.651	0.006	4.945	0.009	3.595	0.011	5.644	0.004	0.003	-	8.000
	5.456	0.004	5.180	0.006	3.899	0.017	5.373	-	0.011	0.014	8.000
	5.264	0.006	5.567	-	3.925	0.010	5.163	0.008	0.002	0.004	8.000
	5.490	-	5.200	0.001	3.774	0.017	5.422	-	0.003	0.004	8.000
	5.637	0.006	4.929	-	3.620	0.015	5.671	0.009	0.004	0.004	8.000
	5.208	0.005	5.743	-	6.029	0.036	2.885	0.005	0.002	0.005	8.000
	5.308	-	5.589	0.005	5.988	0.049	2.947	-	0.021	-	8.000
	5.525	0.006	5.432	0.009	5.573	0.024	3.166	0.007	0.001	0.011	8.000
	5.401	0.009	5.681	0.007	5.436	0.027	3.138	0.017	0.044	0.020	8.000
	5.478	0.004	5.547	0.007	5.591	0.041	3.033	0.019	0.017	0.023	8.000
	6.113	0.081	4.018	0.004	3.529	0.032	5.948	0.045	0.002	0.048	8.000
	6.050	0.065	4.012	0.001	3.468	0.033	6.194	0.038	0.006	0.024	8.000
Carbonate	Si	Ti	Al	Cr	Fe	Mn	Mg	Ca	Na	K	**Total**
6 oxygènes	0.003	0.002	-	-	0.008	0.008	0.004	5.970	0.003	-	-
	0.021	0.003	0.008	-	0.101	0.138	0.045	5.654	0.003	0.003	-
	0.001	-	0.001	-	0.118	0.149	0.055	5.671	0.004	0.004	-
	-	-	-	-	0.095	0.122	0.041	5.739	0.001	0.002	-
	-	0.002	0.004	-	0.104	0.145	0.039	5.701	-	0.002	-
	0.002	-	-	-	0.119	0.155	0.057	5.665	-	-	-
	0.008	-	-	-	1.154	0.370	1.391	3.066	0.005	0.002	-
Epidote	Si	Ti	Al	Cr	Fe	Mn	Mg	Ca	Na	K	**Total**
13 (O. OH)	3.237	0.008	2.304	-	0.915	0.008	0.004	2.126	0.002	0.001	-
	3.234	0.004	2.267	-	0.938	0.008	0.001	2.175	-	-	-
	3.272	0.008	2.244	0.002	0.951	0.005	-	2.111	0.007	-	-
	3.256	0.005	2.212	0.002	0.993	0.005	-	2.159	-	0.002	-
	3.257	0.010	2.214	0.001	0.997	0.006	-	2.138	0.004	-	-
Amphibole	Si	Ti	Al	Cr	Fe	Mn	Mg	Ca	Na	K	**Total**
	7.748	0.029	0.340	-	(1.071)	0.022	3.790	1.858	0.128	0.007	14.992
	7.443	0.027	0.579	0.002	(1.151)	0.031	3.767	1.731	0.134	0.021	14.886
	7.522	0.038	0.555	0.005	(1.341)	0.024	3.514	1.759	0.143	0.016	14.918

4.4. Hydrothermal Alteration and Mineralization

Using some common metals in mineralization such as copper, gold, silver, molybdenum, lead, zinc in association with some indices such as CCPI, AI and IP, it is possible to correlate the mineralization and hydrothermal alteration types.

Factor 1 shows an association of copper, silver, gold, molybdenum, selenium

and antimony mineralization with CCPI and AI (Figure 9(A)). In factor 5 the same mineralization shows a positive correlation with CCPI, TOT/S, FeO_3, and TiO_2 and a negative correlation with AI (Figure 9(E)). In factor 2, the initial mineralization shows a negative correlation with the phenomena. On the other hand, zinc, nickel, barium mineralization is identified and shows a positive correlation with CCPI (Figure 9(B)). Factor 3 translates a positive correlation of copper and gold with the phenomena to which a strong positive correlation with alkaline minerals (Rb, Cs, IP) can be associated. The positive correlation with AI and negative with CCPI is also remarkable (Figure 9(C)). Factor 4 shows an association of gold and silver positively correlated with the phenomenon, as well as AI where the correlation is positive, but negative with CCPI (Figure 9(D)). Factor 6 is quite similar to factor 4 but differs by a negative correlation of the mineralization with gold, silver, selenium with the phenomena (Figure 9(F)). In the four factors where the mineralization with Cu, Au, Ag shows a positive correlation with the different phenomena, Sr on the other hand shows a negative correlation.

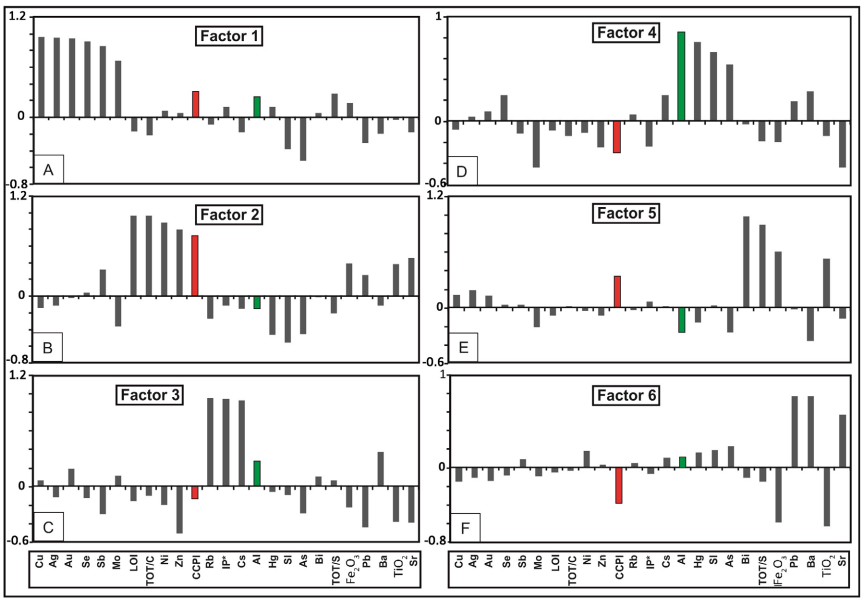

Figure 9. Diagram showing the different factors associated with metals, hydrothermal minerals and alteration index. Evident association of Cu-Au mineralization with alteration indexes is observed in Factors 1 (A), 3 (C) and 5 (E). Factors 2 and 6 show lack of correlation of Cu-Au mineralization with the phenomena (B) (F), whereas, factor 4 shows an association of AI with Se, Au and Ag (D).

The sulfide isotopes for four samples of pyrite are listed in Table 5. The samples consist of one semi-massive pyrite in fractures of quartz veins with few chalcopyrite inclusions which exhibits negative $\delta^{34}S$ sulfide (−4,1) for the pyrite. The three other samples consist of disseminated pyrite associated with hydrothermal minerals (carbonates ± chlorite ± epidote). In these sulfides, the $\delta^{34}S$ values range from 2.5 to 4.7.

Table 5. Result of $\delta^{34}S$ analyses of four samples of Diénéméra-Gongondy deposit.

SAMPLES	Mineral	type	34S
E15D	Pyrite-chalcopyrite	Semi massive	−4.1
E33G	Pyrite	Dissemination	2.5
E39D	Pyrite	Dissemination	4.1
E40D	Pyrite	Dissemination	4.7

5. Discussion

5.1. Hydrothermal Alteration and Mineralization

The use of factor analysis of hydrothermal alteration and mineralization highlighted the association of mineralization and hydrothermal alteration. Indeed, six phenomena are highlighted. The first phenomenon, related to factor 1 correspond to propylitic alteration associated with the Cu-Au-Ag-Mo-Sb mineralization in dioritic intrusions. The same mineralization association is observed in the factor 5 which could be related with phyllitic-carbonate alteration and basic mineralized intrusions represented by microgabbro. The sericitic alteration consists of two types. The first one is represented by factor 3 which is associated with Cu-Au-Mo mineralization and is remarkable by a positive correlation with IP, Rb, Cs and AI. The second is associated with Au-Ag mineralization and Hg, As and SI. This phenomenon can be associated with late orogenic mineralization highlighted by previous studies in the zone [29]-[31]. The last two factors are not associated with the Cu-Au mineralization. The first can be associated with the chloritic alteration regarding the positive correlation with CCPI and negative correlation with AI. The factor 6 corresponds to late non altered diorite which is barren in Cu-Au mineralization. This analysis is in accordance with the ore microscopy studies of the copper mineralization and the study of the hydrothermal alteration at microscopic scale.

The ore microscopy indicated that copper mineralization is associated with hydrothermal alteration. The chalcopyrite is observed in dissemination and associated with alteration minerals, dominated by chlorite and carbonates at Gongondy. However, at Diénéméra, chlorite, carbonates, epidote and muscovite are the most frequent alteration minerals which are associated with dioritic rocks (**Figure 10(A)** and **Figure 10(B)**).

In felsic grinding zones, it can be found in subautomorphic crystals and cemented by felsic recrystallization products including carbonates and silica. Moreover, chalcopyrite is also frequently associated with pyrite in crushing zones (**Figure 10(C)**) or in the form of a trail associated with chlorite and carbonates (**Figure 10(D)**). The fine crystals are most often crumbled or chamoised while the coarser ones are cracked and filled with chlorite which often acts as cement (**Figure 10(E)**). In intergranular interstices in dioritic rocks at Diénéméra, chalcopyrite and pyrite are frequently associated with chlorite, carbonates, epidote and muscovite (**Figure 10(F)**).

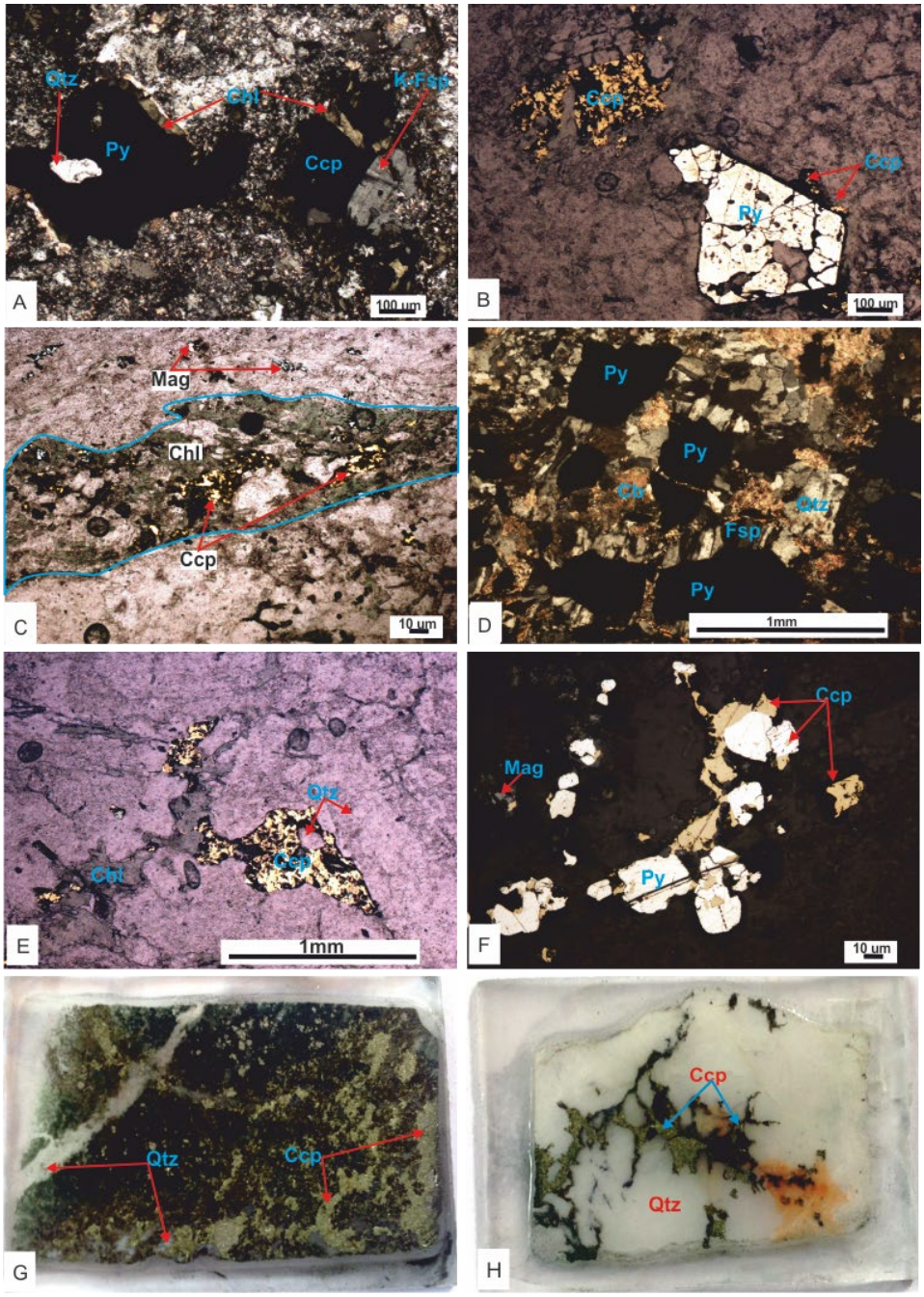

Figure 10. Hand specimens and photomicrographs showing the association of sulfides with hydrothermal alteration. The ore microscopy showed a relation between chalcopyrite and pyrite with some quartz in inclusions in pyrite fractures (A). Sulfides in relation with chlorite and cristal of K-feldspar (B). Defromed and fragmented chalcopyrite associated with chloritic alteration (C). Fragmented pyrite in deformed zone associated with quartz in shadow pressure and carbonate (D). Massive chalcopyrite in quartz fractures (E). Chalcopyrite and pyrite observed in intergranular joint observed in quartz microdiorite (F). Silicified microdiorite associated with semi-massive sulfides (G). Fractured quartz with sulfides in the fractures (H).

In silicified zones, chalcopyrite and pyrite are massive to semi-massive associated with silica and chlorite.

5.2. Lack of Potassic Alteration

The study of Gaoua Porphyry copper deposit showed that potassic alteration is absent. The greenschist facies metamorphism or late hydrothermal alteration can explain this lack, regarding the intense albitization of potassic feldspar and possible chloritization of hydrothermal biotite. The albitization is highlighted by microprobes analyses which indicated that the feldspars in the study area have a composition of albite. Even if [21] thought that this albitization can be related to the chemical factor of Precambrian rock composition, we think that this albitization can be associated with late hydrothermal alteration, notably the propylitic alteration generally associated with albitic phase or with retrograde greenschist facies metamorphism. This latter hypothesis can be justified by the posteriority of potassic alteration in relation with the deposition of the porphyry copper deposit around 2161 ± 23 Ma, whereas the greenschist facies metamorphism occurred during the D2Ga deformational phase which took place after −2150 Ma [28] [30] [32] [58].

5.3. Indicator Minerals

The most important alteration minerals frequently associated with the copper mineralization of Gaoua porphyry copper deposit consists of chlorite, carbonates and locally silica, sericite and epidote. The composition of some of these hydrothermal minerals such as chlorite and epidote is an important tool for porphyry copper mineralization exploration [59]-[63]. The analyses of chlorite in the study area enabled us to define two types of chlorite which are low-magnesium chlorite and the relatively high iron-magnesium chlorite, respectively with Ripidiolite and pycnochlorite composition. The composition of chlorite can permit to discriminate the two chlorites and to see the link of these chlorites with the mineralization. Based on its association and other minerals such as epidote, carbonates and sericite, we classify chlorite depending on the propylitic, phyllitic-carbonates and chlorite alteration zones. In this study, Fe and Mg rich chlorite is found in propylitic alteration zone, possibly in phyllito-carbonates alteration zone, whereas, the low Mg chlorite is observed in the chloritic alteration zone where no relation was observed with the mineralization. In some parts of Diénéméra area, the relatively high Mg content of secondary amphibole (actinolite), associated with chlorite and epidote is a proof of origin of Fe-Mg-chlorite in link with the propylitic alteration. This is in accordance with the chlorite study in Naruo porphyry copper deposit [64] where the binary MgO versus FeO diagram determinated a porphyry copper origin of Mg-chlorite. However, Fe-rich chlorite can be associated with a late fluid, notably in relation with greenschist facies metamorphism or orogenic gold mineralization event which overprinted on the porphyry copper mineralization [28] [29]. The presence of Fe-rich dolomite associated with chlorite can permit to confirm this hypothesis regarding the absence of carbonates in greenschist metamorphic facies [65] [66].

5.4. Potentiality of Cu Mineralization

Alkalis such as Sr, Cs, Rb are the most important trace elements to evaluate the impact of hydrothermal fluids on rocks. The mobility of alkalis due to hydrothermal alteration, the primitive mantle normalized formula of Leach and Campbell [47] (Cs + Rb)/Th can be used as alteration index to determine the potential mineralization of a lithology. According to this formula, most of the samples analyzed, show a value of (Cs + Rb)/Th of more than 5 units confirming the potentiality of Diénéméra-Gongondy mineralization (**Figure 11(A)**).

In the binary diagram of [67] based on the excess of Aluminium content of plagioclase used to determine the fertility of the intrusions, all of the samples fell in the field of fertile intrusion porphyry (**Figure 11(B)**). The clinozoisite composition of epidote is also a proof of the Al-rich origin of plagioclase in the area zone.

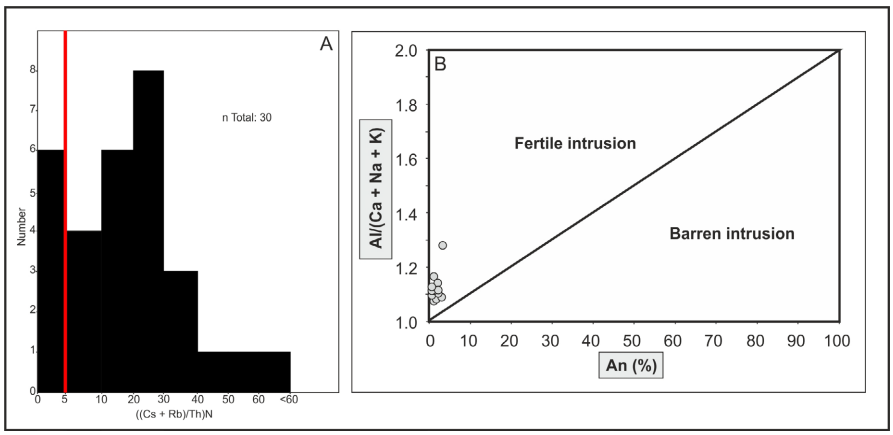

Figure 11. Graph of potential mineralisation index using the primitive mantle normalized formula of [47]. The red line corresponds to limit of potential mineralization which must be more than 5 units (A). Binary diagram of [66] for the determination of the fertility of intrusions. Most of the samples fell in the fertile intrusion field (B).

5.5. Origin of the Fluids

The preliminary δ^{34}S sulfide value of Diénéméra-Gongondy Cu-Au deposit is close to the δ^{34}S mantle value and confirms the magmatic origin of the copper and gold mineralization in comparison with other porphyry copper in the world (**Figure 12**). Indeed, this conclusion is in accordance with studies of fluid inclusions in quartz associated with the mineralization in the study area [28] [30]. The early mineralization is disseminated associated with dioritic intrusions. During the emplacement of the preserved-structure Fe-rich (magnetite) microgabbro and the possible contact with meteoric groundwater induced a probably sericitic alteration and precipitation of copper mineralization, which corroborates with the study of [68]. The emplacement of several generations of late diorites in the form of dykes and especially of a late gabbro adjacent to the mineralization at Diénéméra and Gongondy, could be the origin of the mobilization of hydrothermal fluids rich in iron and magnesium which caused the chloritic alteration observed in certain zones. It is not excluded that this chloritic alteration often associated

with carbonates in relation with the emplacement of the orogenic gold mineralization.

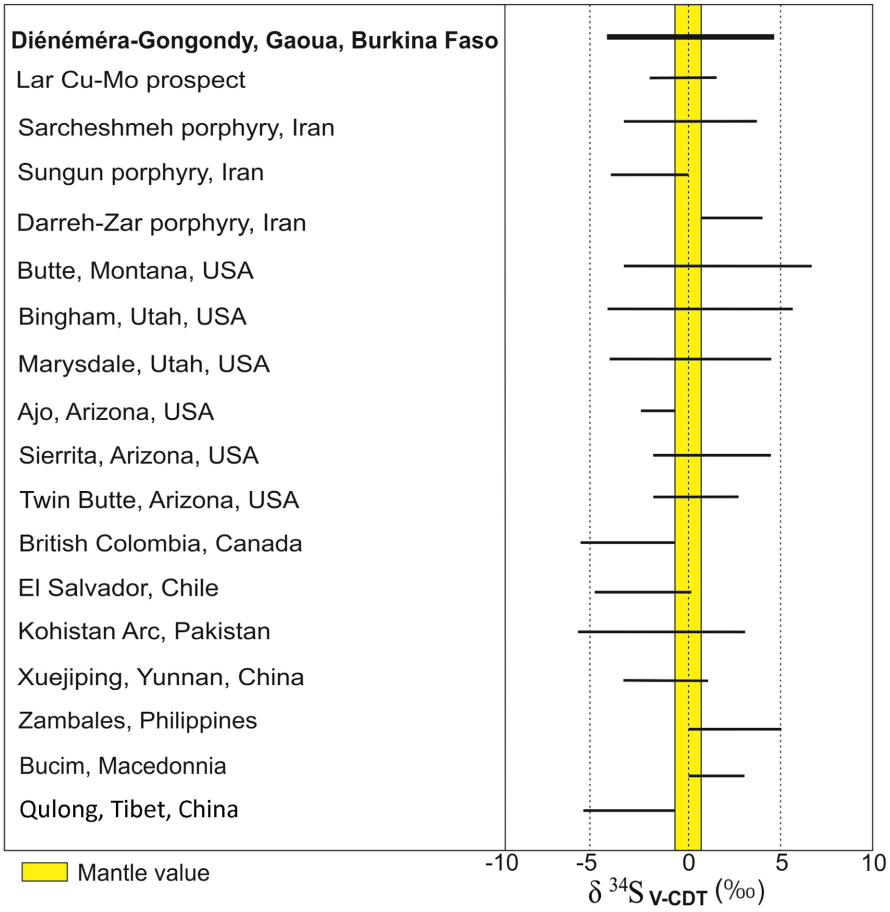

Figure 12. Comparison of the δ34S compositions in the Diénéméra-Gongondy Cu-Au deposit with the other well-known porphyry Cu deposits. Data from [70].

The late fluid which caused the chloritic alteration and released acidic fluids, origin of the dissolution of the rock and carbonates and sulfates filled cavities or breccia. The acidic fluids are the result of interaction of late fluids with the host rocks, responsible of the alteration of albite into chlorite with liberation of acidic fluids according to [69].

The mineralization of Gaoua is however fortunate to have been preserved despite the different phases of late intrusions and the level of erosion that could have destroyed a part of the mineralization. Although the association of copper mineralization with propylitic alteration in Diénéméra is obvious, it does not contradict the conclusions of [1] who defined the propylitic zone as barren. Indeed, the propylitic zone is characterized by disseminated mineralization, and does not constitute an important zone of economically valuable mineralization because the grades are generally low, less than 0.2% of copper. However, the presence of significant mineralization associated with breccia, cavities, intergranular interstices and silicification (**Figure 10**), reflects a last-stage phenomenon that would be the

cause of the remobilization of the copper mineralization or the reconcentration of this mineralization as [25] had stated. The first-order structures associated with the D3Ga deformation phase would have effectively contributed to this remobilization by channeling the fluids rich in gold and copper released by mafic intrusions (Microgabbro) into more permeable and lower pressure zones or zones likely to contain the mineralization such as intergranular interstices, breccia zones or cavities (**Figure 13**) This conclusion is in accordance with studies of Cu-Au-Mo in Oyu Tolgoï [71] [72] and Cu ± Mo ± Au ± Ag in Imourkhssen [73].

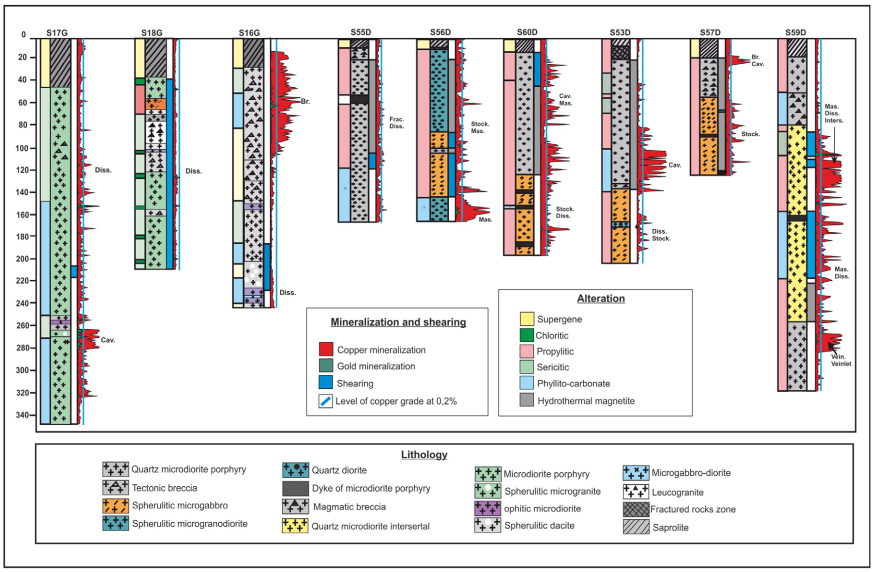

Figure 13. Lithological log of drill cores from Diénéméra and Gongondy deposits showing the relationships between lithologies, copper and gold mineralization, hydrothermal alteration and shearing. Important mineralization (more than 0.2% of copper) can be observed in breccia, cavities, veins and veinlets, intergranular interstices or as massive patches. Abbreviations: Br.: Breccia, Cav.: Cavities, Diss.: Dissemination, Frac.: Fracture, Inters. Intergranular joints, Mas.: Massive, Stock.: Stockwerk.

6. Conclusions

The Diénéméra-Gongondy Cu-Au deposit is a Paleoproterozoic porphyry copper deposit in the West African Craton (WAC). The mineralization is associated with an intrusion complex dominated by dioritic composition with a variable texture.

The petrographic observations and geochemical analyses revealed that the mineralization is associated with the hydrothermal minerals as well as the alteration indexes. Indeed, the copper mineralization is generally associated with some hydrothermal minerals including Mg-Fe-rich chlorite, sericite, carbonates, silica in dissemination, associated with intergranular interstices, breccia or as massive patches. The hydrothermal alterations associated with mineralization are dominated by propylitic alteration in Diénéméra and phyllitic-carbonate alteration in Gongondy. The presence of potassic alteration is not clearly observed. This is probably due to the late-stage albitization associated with retrograde metamorphism or late-stage hydrothermal alteration related to an orogenic gold deposition

which overprinted the porphyry copper-gold deposit. Nevertheless, the potential of porphyry copper mineralization is clearly demonstrated even if the late phenomena have attempted to modify or remobilize the copper-gold mineralization as it is the case in many Paleoproterozoic porphyry copper deposits in the world.

Conflicts of Interest

The authors declare no conflicts of interest regarding the publication of this paper.

References

[1] Sillitoe, R.H. (2010) Porphyry Copper Systems. *Economic Geology*, **105**, 3-41. https://doi.org/10.2113/gsecongeo.105.1.3

[2] Dilles, J.H. and John, D.A. (2021) Porphyry and Epithermal Mineral Deposits. In: Alderton, D. and Elias, S.A., Eds., *Encyclopedia of Geology*, Elsevier, 847-866. https://doi.org/10.1016/b978-0-08-102908-4.00005-9

[3] Chiaradia, M. (2013) Copper Enrichment in Arc Magmas Controlled by Overriding Plate Thickness. *Nature Geoscience*, **7**, 43-46. https://doi.org/10.1038/ngeo2028

[4] Lee, C.A. and Tang, M. (2020) How to Make Porphyry Copper Deposits. *Earth and Planetary Science Letters*, **529**, Article ID: 115868. https://doi.org/10.1016/j.epsl.2019.115868

[5] Chen, H. and Wu, C. (2020) Metallogenesis and Major Challenges of Porphyry Copper Systems above Subduction Zones. *Science China Earth Sciences*, **63**, 899-918. https://doi.org/10.1007/s11430-019-9595-8

[6] Richards, J.P. (2003) Tectono-Magmatic Precursors for Porphyry Cu-(Mo-Au) Deposit Formation. *Economic Geology*, **98**, 1515-1533. https://doi.org/10.2113/98.8.1515

[7] Richards, J.P. (2005) Cumulative Factors in the Generation of Giant Calc-Alkaline Porphyry Cu Deposits. In: Porter, T.M., Ed., *Super Porphyry Copper & Gold Deposits: A Global Perspective*, PGC Publishing, Vol. 1, 7-25.

[8] Richards, J.P. (2011) High Sr/Y ARC Magmas and Porphyry Cu Mo Au Deposits: Just Add Water. *Economic Geology*, **106**, 1075-1081. https://doi.org/10.2113/econgeo.106.7.1075

[9] Vigneresse, J., Truche, L. and Chattaraj, P.K. (2014) Metal (Copper) Segregation in Magmas. *Lithos*, **208**, 462-470. https://doi.org/10.1016/j.lithos.2014.09.025

[10] Sun, W., Huang, R., Li, H., Hu, Y., Zhang, C., Sun, S., *et al.* (2015) Porphyry Deposits and Oxidized Magmas. *Ore Geology Reviews*, **65**, 97-131. https://doi.org/10.1016/j.oregeorev.2014.09.004

[11] Sun, W., Wang, J., Zhang, L., Zhang, C., Li, H., Ling, M., *et al.* (2016) The Formation of Porphyry Copper Deposits. *Acta Geochimica*, **36**, 9-15. https://doi.org/10.1007/s11631-016-0132-4

[12] Liu, H., Liao, R., Zhang, L., Li, C. and Sun, W. (2019) Plate Subduction, Oxygen Fugacity, and Mineralization. *Journal of Oceanology and Limnology*, **38**, 64-74. https://doi.org/10.1007/s00343-019-8339-y

[13] Goldfarb, R.J., André-Mayer, A., Jowitt, S.M. and Mudd, G.M. (2017) West Africa: The World's Premier Paleoproterozoic Gold Province. *Economic Geology*, **112**, 123-143. https://doi.org/10.2113/econgeo.112.1.123

[14] Kolb, J. and Petrov, N. (2016) The Guelb Moghrein Cu-Au Deposit: Neoarchaean Hydrothermal Sulfide Mineralization in Carbonate-Facies Iron Formation. *Ore Geology Reviews*, **78**, 573-577. https://doi.org/10.1016/j.oregeorev.2015.09.003

[15] Schwartz, M.O. and Melcher, F. (2003) The Perkoa Zinc Deposit, Burkina Faso. *Economic Geology*, **98**, 1463-1485. https://doi.org/10.2113/gsecongeo.98.7.1463

[16] Béziat, D., Siebenaller, L., Salvi, S. and Chevalier, P. (2016) A Weathered Skarn-Type Mineralization in Ivory Coast: The Ity Gold Deposit. *Ore Geology Reviews*, **78**, 724-730. https://doi.org/10.1016/j.oregeorev.2015.07.011

[17] Masurel, Q., Thébaud, N., Miller, J., Ulrich, S., Hein, K.A.A., Cameron, G., *et al.* (2017) Sadiola Hill: A World-Class Carbonate-Hosted Gold Deposit in Mali, West Africa. *Economic Geology*, **112**, 23-47. https://doi.org/10.2113/econgeo.112.1.23

[18] McFarlane, C.R.M., Mavrogenes, J., Lentz, D., King, K., Allibone, A. and Holcombe, R. (2011) Geology and Intrusion-Related Affinity of the Morila Gold Mine, Southeast Mali. *Economic Geology*, **106**, 727-750. https://doi.org/10.2113/econgeo.106.5.727

[19] Ilboudo, H., Sawadogo, S., Traoré, A.S., Sama, M., Wenmenga, U. and Lompo, M. (2018) Intrusion-Related Gold Mineralization: Inata Gold Deposit, Bélahourou District, Northern Burkina Faso (West-Africa). *Journal of African Earth Sciences*, **148**, 52-58. https://doi.org/10.1016/j.jafrearsci.2018.05.015

[20] Masurel, Q., Thébaud, N., Allibone, A., André-Mayer, A., Hein, K.A.A., Reisberg, L., *et al.* (2019) Intrusion-Related Affinity and Orogenic Gold Overprint at the Paleoproterozoic Bonikro Au-(Mo) Deposit (Côte d'ivoire, West African Craton). *Mineralium Deposita*, **57**, 557-580. https://doi.org/10.1007/s00126-019-00888-2

[21] Gossens, P.J. (1970) Guide sur la recherche de gisements de Cu/Mo disséminés-type «porphyry copper» en Haute-Volta. PNUD.

[22] Sillitoe, R.H. (1973) An Examination of Porphyry Copper-Molybdenum Prospects and the Overall Metallogeny of the Birrimian System in Upper Volta and Niger, West Africa.

[23] Sillitoe, R.H. (2007) An Appraisal of the Dienemera and Gongondy Copper-Gold Prospects, Gaoua District, Burkina Faso. Wentworth Resources Pty Ltd., 16 p.

[24] Sillitoe, R.H. (2008) Geological Modelling of Dienemera and Gongondy Breccia-hosted Copper-Gold Prospects, Gaoua District, Burkina Faso. Wentworth Resources Pty Ltd., 11 p.

[25] Gamsonré, P.E. (1970) Etude pétrologique et métallogénique de la région de Gongondy, Diénéméra et Malba. Thèse de 3e cycle, Univ. Besançon, Fr., 249 p.

[26] Sougue, P. (1985) Rapport technique détaillé sur les sondages carottés dans le secteur de Diénéméra Nord. PMG.

[27] Naré, A. (2011) Métallogénie du cuivre-or de Gaoua, Sud-Ouest du Burkina Faso, Afrique de l'Ouest. Master Prof., Université de Toulouse, 56 p.

[28] Mignot, E.L., Siebenaller, L., Béziat, D., Salvi, S., Andrémayer, A., Reisberg, L., *et al.* (2014) The Paleoproterozoic Copper-Gold Deposit of Gaoua, Burkina Faso: Evidence for a Polyphased Mineralization. *Acta Geologica Sinica—English Edition*, **88**, 970-972. https://doi.org/10.1111/1755-6724.12378_5

[29] Le Mignot, E., Siebenaller, L., Béziat, D., André-Mayer, A., Reisberg, L., Salvi, S., *et al.* (2017) The Paleoproterozoic Copper-Gold Deposits of the Gaoua District, Burkina Faso: Superposition of Orogenic Gold on a Porphyry Copper Occurrence? *Economic Geology*, **112**, 99-122. https://doi.org/10.2113/econgeo.112.1.99

[30] Baratoux, L., Metelka, V., Naba, S., Ouiya, P., Siebenaller, L., Jessell, M.W., *et al.* (2015) Tectonic Evolution of the Gaoua Region, Burkina Faso: Implications for Mineralization. *Journal of African Earth Sciences*, **112**, 419-439. https://doi.org/10.1016/j.jafrearsci.2015.10.004

[31] Siebenaller, L., Béziat, D., Salvi, S., Naba, S., Le Mignot, E., Baratoux, L., *et al.* (2015)

WITHDRAWN: The Gaoua Porphyry Cu-Au Deposit, SW Burkina Faso. *Ore Geology Reviews*. https://doi.org/10.1016/j.oregeorev.2015.10.031

[32] André-Mayer, A.-S., Cathelineau, M., Muchez, P., Pirard, E. and Sindern, S. (2015) Mineral Resources in a Sustainable World. *Proceedings of the* 13*th Biennial SGA Meeting*, Nancy, 24-27 August 2015, 2134 p.

[33] Hallarou, M.M., Konaté, M., Olatunji, A.S., Ahmed, Y., Ajayi, F.F. and Abdul, R.M. (2020) Re-Os Ages for the Kourki Porphyry Cu-Mo Deposits, North West Niger (West Africa): Geodynamic Implications. *European Journal of Environment and Earth Sciences*, **1**, 1-13. https://doi.org/10.24018/ejgeo.2020.1.4.43

[34] SRK Consulting Ltd. (2013) Technical Report on a Mineral Resource Estimation for the Gaoua Project, Burkina Faso. 150 p.

[35] PNUD (1970) Enquête sur les ressources minières et les ressources en eaux souterraines en Haute Volta.

[36] Kahou, Z.S., Duchêne, S., Brichau, S., Campos, E., Estrade, G., Poujol, M., *et al.* (2021) Mineralogical and Chemical Characterization of Supergene Copper-Bearing Minerals: Examples from Chile and Burkina Faso. *Ore Geology Reviews*, **133**, Article ID: 104078. https://doi.org/10.1016/j.oregeorev.2021.104078

[37] Kouamelan, A.N., Delor, C. and Peucat, J. (1997) Geochronological Evidence for Reworking of Archean Terrains during the Early Proterozoic (2.1 Ga) in the Western Coˆte D'ivoire (Man Rise-West African Craton). *Precambrian Research*, **86**, 177-199. https://doi.org/10.1016/s0301-9268(97)00043-0

[38] Boher, M., Abouchami, W., Michard, A., Albarede, F. and Arndt, N.T. (1992) Crustal Growth in West Africa at 2.1 Ga. *Journal of Geophysical Research*: *Solid Earth*, **97**, 345-369. https://doi.org/10.1029/91jb01640

[39] Baratoux, L., Metelka, V., Naba, S., Jessell, M.W., Grégoire, M. and Ganne, J. (2011) Juvenile Paleoproterozoic Crust Evolution during the Eburnean Orogeny (~2.2-2.0 Ga), Western Burkina Faso. *Precambrian Research*, **191**, 18-45. https://doi.org/10.1016/j.precamres.2011.08.010

[40] Metelka, V., Baratoux, L., Naba, S. and Jessell, M.W. (2011) A Geophysically Constrained Litho-Structural Analysis of the Eburnean Greenstone Belts and Associated Granitoid Domains, Burkina Faso, West Africa. *Precambrian Research*, **190**, 48-69. https://doi.org/10.1016/j.precamres.2011.08.002

[41] Van De Steen, J. and Sattran, V. (1982) Recherches géologiques et minières dans les sillons de Houndé et de Boromo. Rapport final technique de synthèse. PNUD projet UPV 74-004, 124 p.

[42] Naba, S. (2010) Rapport final d'une étude pétrostructurale de la zone exclue dans le permis de Gaoua Minerals à l'est de Gaoua. Volta Resources, 64 p.

[43] Belemsobgo, A., Zongo, W.P.P., Wenmenga, U. and Naba, S. (2024) Fertilité des intrusions dans les porphyres cuprifères paléoprotérozoïques de la ceinture de roches vertes birimienne de Boromo, Burkina Faso, Craton Ouest Africain. *Afrique Science*, **24**, 60-74.

[44] Brownscombe, W. (2009) The Tinga Anomaly: A New Style of Gold Mineralization in Ghana? University of Oxford, 80 p.

[45] Ishikawa, Y., Sawguchi, T., Iwaya, S. and Horiuchi, M. (1976) Delineation of Prospective Targets for Kuroko Deposits Based on Modes of Volcanism of Underlying Dacite and Alteration Halos. *Mining Geology*, **26**, 105-117.

[46] Large, R.R. (2001) The Alteration Box Plot: A Simple Approach to Understanding the Relationship between Alteration Mineralogy and Lithogeochemistry Associated with

Volcanic-Hosted Massive Sulfide Deposits. *Economic Geology*, **96**, 957-971. https://doi.org/10.2113/96.5.957

[47] Heath, C.J. and Campbell, I.H. (2004) A New Geochemical Technique for Gold Exploration: Alkali Element Mobility Associated with Gold Mineralization in the West Australian Goldfields. *Economic Geology*, **99**, 313-324. https://doi.org/10.2113/gsecongeo.99.2.313

[48] Hughes, C.J. (1972) Spilites, Keratophyres, and the Igneous Spectrum. *Geological Magazine*, **109**, 513-527. https://doi.org/10.1017/s0016756800042795

[49] Trepanier, S. (2011) Guide pratique d'utilisation des différentes méthodes de traitement de l'altération et du métasomatisme. Consorem, UQAC.

[50] Van Gerven, M. (1995) Geochemische Nebengesteins Alterationen and Erfassung Signifi kanter Zonierungen im Bereich des Jade-Erzfeldes, Okinawa, Trog, Japan. Ph.D. Thesis, Freir Universitate, Rohstoff and Umweltgeologie, 186.

[51] Guo, N., Guo, W., Shi, W., Huang, Y., Guo, Y. and Lian, D. (2020) Characterization of Illite Clays Associated with the Sinongduo Low Sulfidation Epithermal Deposit, Central Tibet Using Field SWIR Spectrometry. *Ore Geology Reviews*, **120**, Article ID: 103228. https://doi.org/10.1016/j.oregeorev.2019.103228

[52] Deer, W.A., Howie, R. A. and Zussman, J. (1992) An Introduction to the Rock-Forming Minerals. Sheet Silicates. Longman Scientific & Technical/Wiley, 549.

[53] Franz, G. and Liebscher, A. (2004) Physical and Chemical Properties of the Epidote Minerals: An Introduction. *Reviews in Mineralogy & Geochemistry*, **56**, 1-82. https://doi.org/10.1515/9781501509599-004

[54] Trdlicka, Z. and Hoffman, V. (1976) Untersuchungen der chemischen Zusammensetzung der Gangkarbonate von Kutna Hora/CSSR. *Freiberger Forschungshefte*, **321**, 29-81.

[55] Bailey, S.W. (1975) Chlorites. In: Gieseking, J.E., Ed., *Soil Components*, Springer, 191-263. https://doi.org/10.1007/978-3-642-65917-1_7

[56] Leake, B.E. (1971) On Aluminous and Edenitic Hornblendes. *Mineralogical Magazine*, **38**, 389-407. https://doi.org/10.1180/minmag.1971.038.296.01

[57] Leake, B.E., Woolley, A.R., Arps, C.E.S., Birch, W.D., Gilbert, M.C., Grice, J.D., *et al.* (1997) Nomenclature of Amphiboles Report of the Subcommittee on Amphiboles of the International Mineralogical Association Commission on New Minerals and Mineral Names. *European Journal of Mineralogy*, **9**, 623-651. https://doi.org/10.1127/ejm/9/3/0623

[58] Parra-Avila, L.A., Belousova, E., Fiorentini, M.L., Baratoux, L., Davis, J., Miller, J., *et al.* (2016) Crustal Evolution of the Paleoproterozoic Birimian Terranes of the Baoulé-Mossi Domain, Southern West African Craton: U-Pb and Hf-Isotope Studies of Detrital Zircons. *Precambrian Research*, **274**, 25-60. https://doi.org/10.1016/j.precamres.2015.09.005

[59] Cooke, D.R., Hollings, P., Wilkinson, J.J. and Tosdal, R.M. (2014) Geochemistry of Porphyry Deposits. In: Holland, H.D. and Turekian, K.K., Eds., *Treatise on Geochemistry*, Elsevier, 357-381. https://doi.org/10.1016/b978-0-08-095975-7.01116-5

[60] Wilkinson, J.J., Chang, Z., Cooke, D.R., Baker, M.J., Wilkinson, C.C., Inglis, S., *et al.* (2015) The Chlorite Proximitor: A New Tool for Detecting Porphyry Ore Deposits. *Journal of Geochemical Exploration*, **152**, 10-26. https://doi.org/10.1016/j.gexplo.2015.01.005

[61] Wilkinson, J.J., Cooke, D.R., Baker, M.J., Chang, Z., Wilkinson, C.C., Chen, H., *et al.* (2017) Porphyry Indicator Minerals and Their Mineral Chemistry as Vectoring and

Fertility Tools: Geological Survey of Canada. Open File 8345, 67-77.

[62] Wilkinson, J.J., Pacey, A., Hart-Madigan, L.A., Longridge, J., Cooke, D.R., Baker, M.J., *et al.* (2019) A New Paradigm for the Origin of Propylitic Alteration in Porphyry Ore Systems. *Applied Earth Science*, **128**, 64-65. https://doi.org/10.1080/25726838.2019.1607194

[63] Cooke, D.R., Agnew, P., Hollings, P., Baker, M., Chang, Z., Wilkinson, J.J., *et al.* (2020) Recent Advances in the Application of Mineral Chemistry to Exploration for Porphyry Copper-Gold-Molybdenum Deposits: Detecting the Geochemical Fingerprints and Footprints of Hypogene Mineralization and Alteration. *Geochemistry: Exploration, Environment, Analysis*, **20**, 176-188. https://doi.org/10.1144/geochem2019-039

[64] Li, F., Tang, J., Song, Y., Li, S., Tang, P., Li, H., *et al.* (2024) Major Elements Geochemistry of Chlorite in Different Ore Deposits and Its Genesis and Exploration Significance: A Case Study from Naruo Porphyry Cu Deposit in Duolong Ore District, Tibet. *Frontiers in Earth Science*, **12**, Article ID: 1378820. https://doi.org/10.3389/feart.2024.1378820

[65] Djouka-Fonkwe, M.L., Kyser, K., Clark, A.H., Urqueta, E., Oates, C.J. and Ihlenfeld, C. (2012) Recognizing Propylitic Alteration Associated with Porphyry Cu-Mo Deposits in Lower Greenschist Facies Metamorphic Terrain of the Collahuasi District, Northern Chile—Implications of Petrographic and Carbon Isotope Relationships. *Economic Geology*, **107**, 1457-1478. https://doi.org/10.2113/econgeo.107.7.1457

[66] Mathieu, L. (2018) Quantifying Hydrothermal Alteration: A Review of Methods. *Geosciences*, **8**, Article No. 245. https://doi.org/10.3390/geosciences8070245

[67] Williamson, B.J., Herrington, R.J. and Morris, A. (2016) Porphyry Copper Enrichment Linked to Excess Aluminium in Plagioclase. *Nature Geoscience*, **9**, 237-241. https://doi.org/10.1038/ngeo2651

[68] Harris, A.C. and Golding, S.D. (2002) New Evidence of Magmatic-Fluid-Related Phyllic Alteration: Implications for the Genesis of Porphyry Cu Deposits. *Geology*, **30**, 335-338. https://doi.org/10.1130/0091-7613(2002)030<0335:neomfr>2.0.co;2

[69] Robb, L. (2005) Introduction to Ore-Forming Processes. Blackwell Sciences Ltd., 376 p.

[70] Boomeri, M., Moradi, R., Stein, H. and Bagheri, S. (2019) Geology, Re-Os Age, S and O Isotopic Composition of the Lar Porphyry Cu-Mo Deposit, Southeast Iran. *Ore Geology Reviews*, **104**, 477-494. https://doi.org/10.1016/j.oregeorev.2018.11.018

[71] Khashgerel, B.-E., Rye, R.O., Hedenquist, J.W. and Kavalieris, I. (2006) Geology and Reconnaissance Stable Isotope Study of the Oyu Tolgoi Porphyry Cu-Au System, South Gobi, Mongolia. *Economic Geology*, **101**, 503-522. https://doi.org/10.2113/gsecongeo.101.3.503

[72] Porter, T.M. (2016) The Geology, Structure and Mineralisation of the Oyu Tolgoi Porphyry Copper-Gold-Molybdenum Deposits, Mongolia: A Review. *Geoscience Frontiers*, **7**, 375-407. https://doi.org/10.1016/j.gsf.2015.08.003

[73] Ferraq, M., Belkacim, S., Cheng, L., Davies, J.H.F.L., Perrot, M.G., Ben-Tami, A., *et al.* (2024) New Geochemical and Geochronological Constraints on the Genesis of the Imourkhssen Cu±Mo±Au±Ag Porphyry Deposit (Ouzellagh-Siroua Salient, Anti-Atlas, Morocco): Geodynamic and Metallogenic Implications. *Minerals*, **14**, Article No. 832. https://doi.org/10.3390/min14080832